Remote Sens. **2015**, *7*, 14227-14258; doi:10.3390/rs71014227

OPEN ACCESS

remote sensing

ISSN 2072-4292

www.mdpi.com/journal/remotesensing

Article

The Potential of EnMAP and Sentinel-2 Data for Detecting Drought Stress Phenomena in Deciduous Forest Communities

Sandra Dotzler *, Joachim Hill, Henning Buddenbaum and Johannes Stoffels

Environmental Remote Sensing and Geoinformatics, University of Trier, Behringstr. 21, 54286 Trier, Germany; E-Mails: hillj@uni-trier.de (J.H.); buddenbaum@uni-trier.de (H.B.); stoffels@uni-trier.de (J.S.)

***** Author to whom correspondence should be addressed; E-Mail: dotzler@uni-trier.de; Tel.: +49-651-201-4593; Fax: +49-651-201-3815.

Academic Editors: Saskia Foerster, Véronique Carrere, Michael Rast, Karl Staenz, Magaly Koch and Prasad S. Thenkabail

Received: 29 July 2015 / Accepted: 20 October 2015 / Published: 27 October 2015

Abstract: Given the importance of forest ecosystems, the availability of reliable, spatially explicit information about the site-specific climate sensitivity of tree species is essential for implementing suitable adaptation strategies. In this study, airborne hyperspectral data were used to assess the response of deciduous species (dominated by European beech and Sessile and Pedunculate oak) to water stress during a summery dry spell. After masking canopy gaps, shaded crown areas and non-deciduous species, potentially indicative spectral indices, the Photochemical Reflectance Index (PRI), Moisture Stress Index (MSI), Normalized Difference Water Index (NDWI), and Chlorophyll Index (CI), were analyzed with respect to available maps of site-specific soil moisture regimes. PRI provided an important indication of site-specific photosynthetic stress on leaf level in relation to limitations in soil water availability. The CI, MSI and NDWI revealed statistically significant differences in total chlorophyll and water concentration at the canopy level. However, after reducing the canopy effects by normalizing these indices with respect to the structure-sensitive simple ratio (SR) vegetation index, it was not yet possible to identify site-specific concentration differences in leaf level at this early stage of the drought. The selected indicators were also tested with simulated EnMAP and Sentinel-2 data (derived from the original airborne data set). While PRI proved to be useful also in the spatial resolution of EnMAP (GSD = 30 m), this was not the case with Sentinel-2, owing to the lack of adequate spectral bands; the remaining indicators (MSI, CI, SR) were also

successfully produced with Sentinel-2 data at superior spatial resolution (GSD = 10 m). The study confirms the importance of using earth observation systems for supplementing traditional ecological site classification maps, particularly during dry spells and heat waves when ecological gradients are increasingly reflected in the spectral response at the tree crown level. It also underlined the importance of using Sentinel-2 and EnMAP in synergy, as soon as both systems become available.

Keywords: hyperspectral imaging; global warming; drought stress; early detection; spectral indicators; water and chlorophyll concentration; PRI; European beech; EnMAP; Sentinel-2

1. Introduction

Climatic changes seemed to have a generally positive impact on forest productivity when water was not limiting [1]. However, future climate changes are likely to include further increases in mean temperature (about 2–4 °C globally) with significant drying in some regions, as well as increases in frequency and severity of extreme droughts, hot extremes, and heat waves (cf. IPCC new report, [2]). Recent studies of increased tree mortality and die-offs triggered by drought and/or high temperatures suggest that at least some of the world's forested ecosystems may be already responding to climate change. This raises concern that forests may become increasingly vulnerable to higher background tree mortality rates and die-off in response to future warming and drought, even in environments that are not normally considered water-limited [3].

The European Environmental Agency expects forests in Europe to be among the ecosystems most affected by climate change [4]. Examples of recent die-offs have been reported from southern and central parts of Europe (e.g., [5]), and it is expected that forests will become increasingly affected by drought, either during exceptional events or under a long-term drift towards more arid conditions, such as which already prevails in Mediterranean areas. Extreme climatic events, such as the heat wave and drought episode experienced during summer 2003, are expected to occur at increased frequencies [6,7]. Diffuse tree mortality within forest stands, being frequently reported after such extreme events, may be exacerbated by soil properties (mainly local water storage capacity) or genetic diversity among and within tree species [8,9]. Due to the direct impact of heat waves and dry spells, forest ecosystems are also expected to become more susceptible to pests and diseases. These combined effects bear the risk of a reduction of important ecosystem services, such as carbon sequestration, water retention, soil protection, biodiversity and, last but not least, economic value [8,10–12].

Determining which ecologically and economically important tree species will gain or lose congruence with their favorable climatic conditions has been, and still is, attracting substantial attention. Thus, it is widely agreed that our present knowledge about the resilience of tree species towards global warming processes necessitates further research with a particular focus on system-oriented approaches, specific site conditions and management options [13].

The use of advanced remote sensing systems for detecting and monitoring stress phenomena and identifying water-limited forest stands across a wide range of site conditions and considering the current tree species distribution is an innovative and powerful extension of observational studies in the sense of

Reyer *et al.* [14]. It holds a strong potential for improving existing ecological site classification maps, and for identifying priority areas for implementing suitable adaptation strategies (e.g., in terms of replacing sensitive tree species). For example, the regional impact of the exceptionally hot and dry summer of 2003 has been analyzed in various studies [9,15–18]. In the German state of Rhineland-Palatinate, the forests in the Donnersberg region were among the most heavily affected. It was demonstrated that the progression of drought in 2003 could be monitored through spectral indicators derived from calibrated Landsat-5 TM sequences, and that drought stress was not homogeneously distributed but highly variable with respect to ecological site conditions, such as soil water availability and other topographic and microclimatic characteristics [19]. Although measuring and assessing soil water dynamics is crucial, the available spatially explicit information on these conditions is limited and to some extent based on outdated records. In Germany, for example, most of the ecological site classification maps are based on climate records from 1931–1960 and have not yet been updated, nor do they incorporate future climate change projections (e.g., [20]). Therefore, in spite of improved mapping techniques, advances in geospatial data processing and the increasing availability of high resolution digital elevation data, further research is needed until ecological site classification maps with information on soil water availability will be available for extended forest areas.

Although the analysis of flux tower measurements from 2003 suggest that the drop in productivity was not primarily caused by high temperatures but rather by limitation of water [18,21], the question arises of whether remote observations should focus solely on canopy water or include also spectral indicators of photosynthetic stress/activity. Intrinsically coupled to this issue is the question which type of satellite systems, already available or planned, has the capacity to identify the most sensitive stands at an early stage and across topographically variable terrain.

Recently, experimental studies with a hyperspectral imaging system (mounted on a platform in 4 m height) have demonstrated the detectability of water stress in four-year old European Beech seedlings already in an early stage [22–24]. Furthermore, it was also possible to retrieve chlorophyll and water content on leaf images with a spatial resolution in the sub-millimeter range [25]. Additional research combined hyperspectral imaging within the reflective (0.4–2.5 μm) and thermal range (8–14 μm) to compare the response of stressed and non-stressed beech plants under high solar irradiance conditions. It was found that the water-sensitive indicators, Moisture Stress Index (MSI) and Normalized Difference Water Index (NDWI), and the spectral indices sensitive to changes in photosynthetic state, Photochemical Reflectance Index (PRI), were significantly correlated with different stress levels [26].

The prime objective of the study presented here was to understand whether comparable results might also be achieved with forthcoming environmental satellite systems, such as the Sentinel-2 (in orbit since 23 June 2015) [27] and the hyperspectral space mission EnMAP (to be launched in 2018) [28]. It was of particular interest to understand the potential and limitations of both systems in providing spatially explicit information on drought/heat-induced stress phenomena and to test the correspondence between the spatial pattern of detectable stress indicators and available site condition maps. Understanding whether the selected stress indicators are already sensitive at early stages of drought is important, assuming that initially affected stands are located on most limited sites. This involves considerable scale transitions (from beech seedlings/plants kept under controlled conditions to full deciduous canopies in variable terrain and soil conditions).

With respect to the extension (almost 80 km²) and limited accessibility of the study area and the necessity of designing a time-efficient sampling scheme (to be implemented during one of the forthcoming drought events), an additional objective was to investigate whether hyperspectral data can support the identification of suitable sites for collecting biophysical data on leaf level.

2. Materials and Methods

2.1. Study Area

The study area is located in the Donnersberg region in the German state of Rhineland-Palatinate (RLP) (49.62 °N, 7.92 °E, Figure 1). As more than 40% of RLP is covered by forests it is one of most densely wooded states in Germany [29]. The study site extends over an area of about 25 km² in the relatively dry part of RLP and is entirely covered by forests. Main tree species are European beech (*Fagus sylvatica L.*), Sessile oak (*Quercus petraea* (Mattuschka) Liebl.) and Pedunculate oak (*Quercus robur* L.), followed by Scots pine (*Pinus sylvestris* L.), sycamore maple (*Acer pseudoplatanus* L.), and Norway spruce (*Picea abies* (L.) H. Karst.).

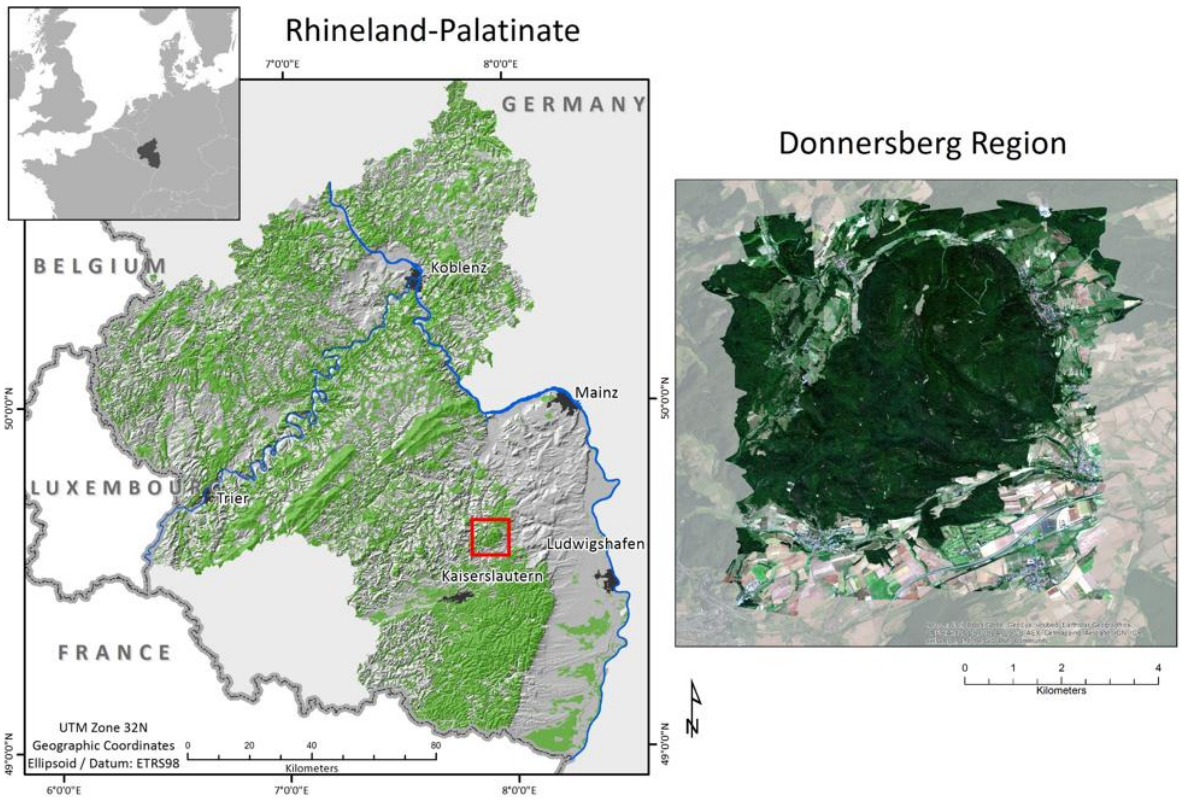

Figure 1. Location of the study area in the German state of Rhineland-Palatinate (**left**). Forested areas are displayed in green. The airborne mosaic of the Donnersberg area acquired on 3 July 2014 is displayed on the **right**.

Soils in the Donnersberg-Rhyolith-Dome are developed on igneous, volcanic rock of silica-rich composition. Owing to the rugged topography with an altitude range of 350–687 m above sea level and slopes of varying orientation, soil depth and corresponding water storage capacities are highly variable and create diverse growth conditions. The climate is generally warm and dry; the annual average temperature

was 9.2 °C in 2014 with a total annual rainfall of 920 mm. However, due to its geographical position east of the Hunsrück mountain range, the area is prone to pronounced dry spells during spring and summer.

2.2. BiomeBGC Simulations

With the objective of identifying optimum periods for acquiring airborne hyperspectral data, the effect of local weather conditions on tree productivity was constantly monitored through the process-based growth model BiomeBGC [30–33]. The model is parameterized with meteorological data from a weather station located in the Donnersberg area; this station has recorded data since mid-2012, such that conditions in 2013 (considered a "normal" or average year) and 2014 could be compared. Based on the climatic record of 2014, net primary productivity (NPP) was simulated with standard/default eco-physiological constants for deciduous broadleaf forest in two scenarios, one with a deep soil of 1 m and one with a shallow soil of 0.5 m.

Figure 2 shows cumulative rainfall and temperature in 2013 and 2014 as well as modelled NPP for both years for a deep and a shallow soil profile. The rainfall and temperature records (Figure 2A,B) demonstrate that in the period before the overflight (black line) less rainfall was received than in 2013, and that spring and early summer in 2014 were much warmer than in 2013. With respect to this period, 2014 was even dryer and warmer than the extreme year 2003. The dashed line marks the day of year (DOY) when 420 °C cumulative temperature is reached which marks the beginning of the growing season.

The corresponding NPP plots (Figure 2C,D) show that the vegetation period started much earlier in 2014. Owing to the water shortage experienced until day of year 180 in 2014, the NPP is clearly reduced on both soil profiles. However, only in the shallow soil scenario negative NPP values indicate that drought-induced stress levels are reached [34]. With respect to good flight conditions, the acquisition of the airborne hyperspectral data was scheduled for 3 July 2014. Due to minor rainfall a few days before the overflight, the stress conditions were then slightly alleviated.

2.3. Soil Moisture Regimes

Analyzing the spectral response of drought-affected tree communities across topographically variable terrain requests suitable reference information. However, collecting a statistically representative sample of leaf-water and pigment concentrations across topographic gradients within the overpass day was technically not feasible. As an alternative strategy, it was decided to compare the spatial pattern of spectrally derived stress indicators with the official digital site classification map (provided by the State Forest Administration). This information layer builds on a long tradition in establishing mapping concepts, and it integrates information on soil depth, texture, bulk density, and soil organic matter with climatological factors and topographic site characteristics (slope, aspect) to provide a qualitative assessment of the soil water balance [20].

The available map (Figure 3) displays a series of soil moisture classes (SMCs) ("Frischestufen"), ranging from "extremely moist" to "extremely dry". The SMCs with a high risk of drying out are located on shallow soils, primarily found on isolated mountain tops, ridges and on sloping terrain (primarily with southerly orientation), while the more favorable locations with sufficient long-term water supply are rather located on plateau areas, lower slopes and in valley bottoms. It should be noted

that under current climate conditions the extremely moist sites were not considered highly suitable due to the risk of waterlogging [35].

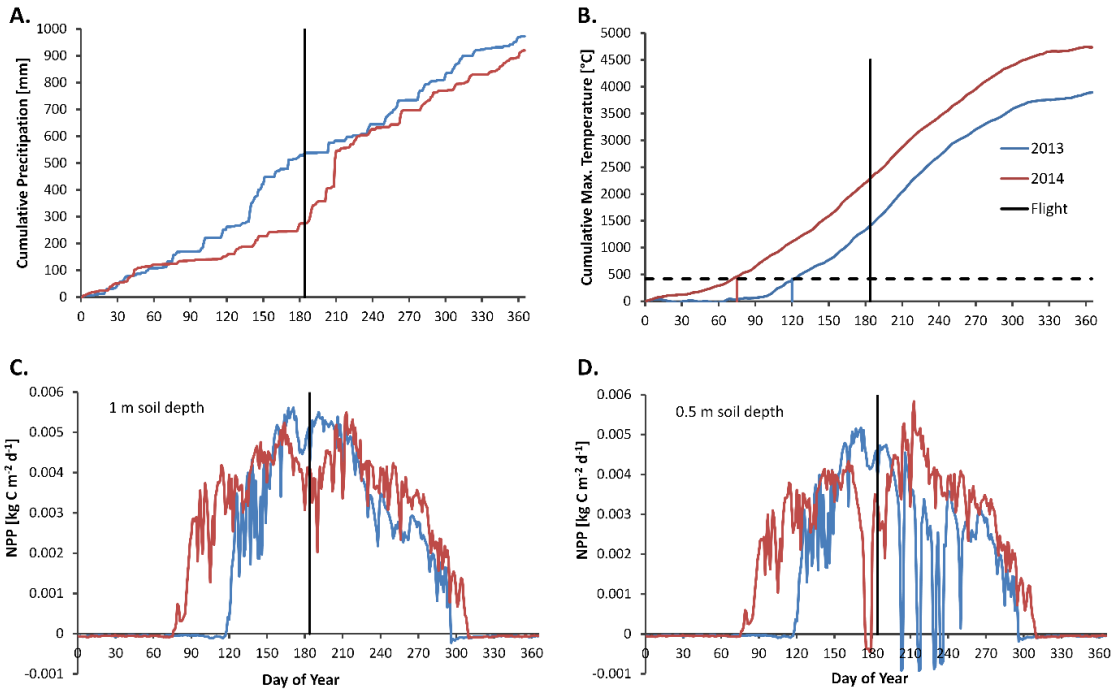

Figure 2. Climate data and BiomeBGC simulations of net primary productivity (NPP) in 2013 (red) and 2014 (blue). The HySpex overflight on day of year 184 is marked by black lines. (**A**) Cumulative precipitation. (**B**) Cumulative daily maximum temperatures. The start of the growing season at 420 ℃ cumulative temperature is marked. (**C**) NPP for 2013 and 2014 for 1 m soil depth and (**D**) 0.5 m soil depth.

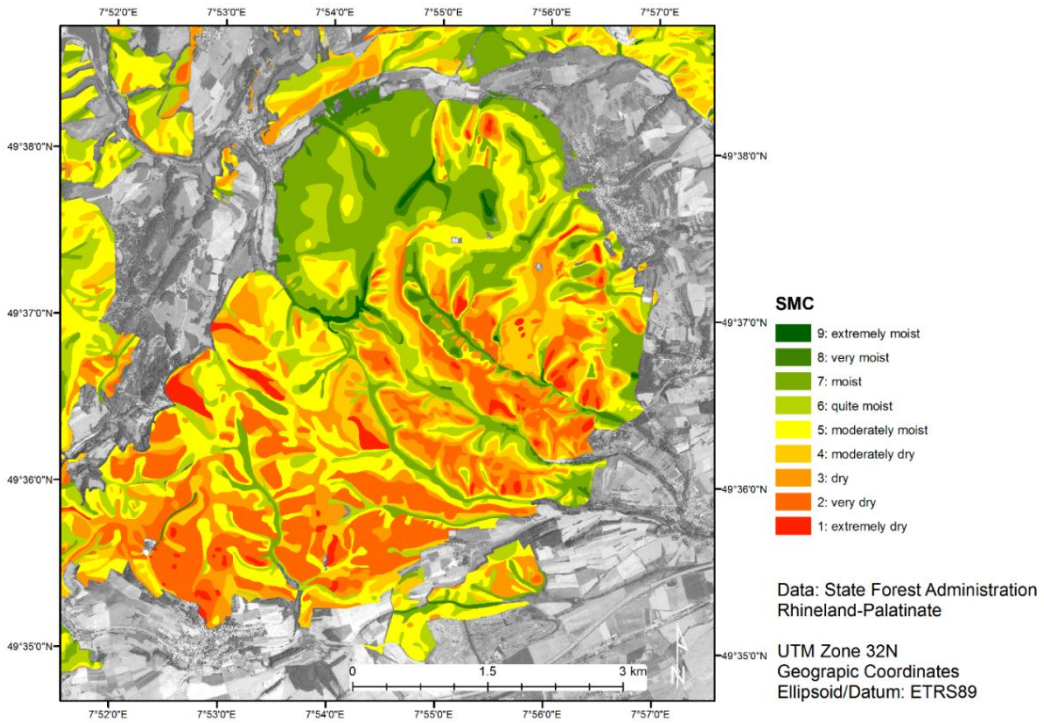

Figure 3. Soil moisture regime classes (SMC) in the Donnersberg region.

Long-term growth rates vary in correspondence to these site conditions. Because the importance of soil water content in the root zone has also been emphasized in several studies on the European drought in 2003 [18,21,36], it is expected that the trees on the dry to very dry SMCs, though better adapted to water shortage, would be the first to exhibit stress phenomena during drought periods. Correspondingly, tree communities in the moist to extremely moist SMCs might be able to maintain high productivity during much of the dry spells.

2.4. Remote Sensing Data

2.4.1. HySpex Airborne Hyperspectral Data

On 3 July 2014, a cloud-free mosaic was recorded with the airborne HySpex sensor (Norsk Elektro Optikk, Skedsmokorset, Norway) of Trier University, mounted on a Cessna 172 aircraft (Figure 1). The imaging spectrometer consists of two camera modules, a module in the visible and near infrared region (VNIR) and a second module in the short wave infrared region (SWIR): the VNIR camera (HySpex VNIR-1600) covers the spectral range from 400–1000 nm with 160 bands at a bandwidth of 3.7 nm, while the SWIR module (HySpex SWIR-320m-e) has 256 spectral bands (6.5 nm spectral bandwidth) in the range from 1000–2500 nm. The image mosaic is composed of 14 flight lines, which were recorded at a flight altitude of 6000 ft. above ground, providing an original ground sampling distance (GSD) of 0.75 m in the VNIR and of 2.5 m in the SWIR spectral range. The acquisition of the 14 flight lines covered a time span from 11:32–12:26 GMT, during which solar zenith and azimuth angles varied from 26.5 °–28.5 ° and 179.9 °–206.7 °, respectively. Since all flight lines were flown in N-S direction and the HySpex cameras (equipped with field-of-view expanders) cover a relatively narrow field-of-view of ±17 °(VNIR) and ±14 °(SWIR), no substantial bi-directional effects are observed.

The time-dependent variation in sun-target-sensor geometry was included in the atmospheric correction of the acquired image lines, which was performed with AtCPro [37], a radiative transfer code originally inspired by the formulation of 5S [38], consecutively upgraded with additional features (e.g., [39,40]), and validated in the context of several studies [41–43]. AtCPro in its present version 6.0 accounts for atmospheric extinction processes as a function of sensor and terrain elevation and provides corrections for atmospheric absorption, scattering, pixel adjacency and terrain-dependent illumination effects.

The HySpex system is interfaced with a global positioning system (GPS) and an inertial measurement unit (IMU). Since no boresight calibration is performed, high-resolution digital orthophotos were used for identifying the required ground control points (GCPs) for each flight line. The parametric geocoding was performed with PARGE (ReSe Applications Schläpfer [44]) and, by including a digital surface model (DSM), produced an ortho-projected image mosaic with a GSD of 2.5 m and 406 spectral bands covering the range between 400 and 2500 nm; few minor data gaps remained at locations with exceptionally strong aircraft roll (Figure 1). This data set is termed "HySpex2.5" and is published under a creative common license [45].

2.4.2. Airborne Laser Scanning

A complete coverage with airborne laser scanning (ALS) data is available. This data set was acquired by the Rhineland Palatinate "State Bureau of Surveying" (LVermGeo) under leaf-off conditions in 2010. The data were delivered as two separate point clouds (filtered ground points and others); the average point density for each data set in forested areas is 3 points per m².

A digital elevation model (DEM) of 1 m spatial resolution was derived from the filtered ground point cloud. Both point clouds were combined, and the maximum value for each 1 m pixel was determined. This thinned point cloud was used to create a digital surface model (DSM) of the area, and a crown height model (CHM) was calculated as the difference between the DSM and DEM. The CHM was resampled to 2.5 m spatial resolution and smoothed using a 3×3 pixel median filter.

The ALS-derived CHM was sampled for all deciduous stands of advanced age (dominant tree species and age class derived from the official forest inventory data base) within the isolated crown areas identified on the HySpex2.5 data set (Section 2.5). Results clearly indicate a steady increase from SMC1 with extremely dry soil conditions to the SMCs with improved soil water storage capacity (Figure 4, right); the remarkably lower crown height in SMC9 (extremely moist) may be due to locations with stagnant moisture (*i.e.*, unfavourable growth conditions). Obviously, the interquartile range is also increasing towards more moist conditions, indicating increasing heterogeneity of the stands. Since this analysis includes only stands of advanced age, it is concluded that the correspondence between tree height and the SMCs is an expression of long-term growth conditions.

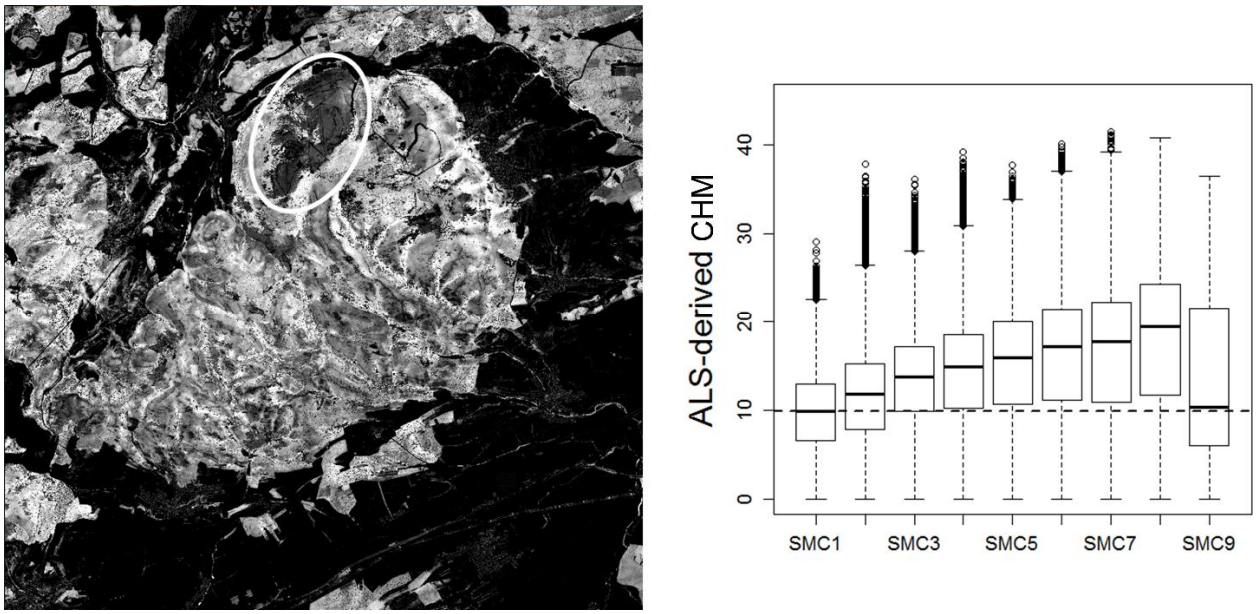

Figure 4. CHM derived from airborne laser scanning in 2010 (**left**) and a boxplot of the deciduous tree heights per SMC (**right**); the encircled area represents an area of extremely dense regrowth after a recent storm damage and, therefore, it has therefore been excluded from the analysis. The boxplots describe the median (black horizontal line inside the "box") of the CHM in each SMC, upper and lower boundary of the box correspond to the 25 and 75% quantile and the end of the whiskers mark the data value which is at maximum 1.5 times the interquartile range from the box (smaller horizontal line at the end of the dashed lines).

2.4.3. Simulated EnMAP and Sentinel-2 Data

The Environmental Mapping and Analysis Program (EnMAP) is a German hyperspectral satellite mission that aims at monitoring and characterizing the Earth's environment on a global scale. EnMAP will cover the range from 420–2450 nm with a spectral sampling of 6.5 nm in the VNIR (420–1000 nm) and 10 nm in the SWIR (900–2450 nm). It will cover a swath of 30 km with 1000 pixels (GSD = 30 m) [28]. For simulating an EnMAP scene over the study area, the HySpex spectra were resampled with EnMAP-compatible Gaussian spectral response functions. After removing the redundant bands in the overlap region between VNIR and SWIR as well as the bands in the region affected by strong atmospheric water vapor (1320–1420 nm and 1795–1950 nm), 209 spectral bands were retained. The geometric characteristics of EnMAP were approximated by filtering the HySpex mosaic with a Gaussian low pass kernel (25 × 25 pixels) and, subsequently, restoring 30 m pixels by calculating the average of all pixels that contribute to the new output pixel size [46,47]. This data set is referred to as "EnMAP30". This data set is masked to the extent of the SWIR module and the forest areas from the SMC map.

Sentinel-2 features 13 spectral bands with 10, 20, and 60 m spatial resolution [27]. The three bands with 60 m resolution are primarily relevant for atmospheric corrections and were not included in this study. Under the assumption that efficient fusion and sharpening algorithms will permit scaling all Sentinel-2 bands to the optimum spatial resolution, Sentinel-2 data was simulated with a common GSD of 10 m. In this case, a Gaussian low-pass filter over a spatial window of 7 × 7 pixels was applied to the airborne mosaic before aggregating the pixels to 10 m GSD. Equivalent Sentinel-2 spectral bands were generated from the HySpex data by applying the appropriate spectral response functions. The data set is termed "Sentinel10".

2.5. Tree Crown Identification

Because stress symptoms in the early phase of a drought period might be expected to produce only subtle spectral variations at the canopy level, it was considered useful to focus the analysis on exclusively illuminated deciduous tree crowns (see also [48]). For eliminating the potentially disturbing influence of shaded crowns and canopy openings with different background materials (e.g., access roads, dry grass, bare soil, exposed rock) from the "HySpex2.5" data set, an approach termed iterative spectral mixture analysis (ISMA) was used.

The ISMA determines the optimum endmember set for unmixing a pixel from large endmember libraries [49] through an iterative approach. The first iteration starts with the full library, and with each subsequent iteration the endmember with the smallest abundance is removed and a new abundance estimate computed, until only one endmember plus "shade" is retained. The optimum endmember set is identified by examining the root-mean-squared-error (RMSE) sequence. While the RMSE continues fluctuating around extremely small values as long as the model is overfitted (*i.e.*, too many endmembers are included in the model, "a" in Figure 5A), it will drastically increase as soon as one of the actually required endmembers is removed ("b"). The optimum set for unmixing the spectral signature then corresponds to the previous iteration (red circle in Figure 5B).

The spectral library with 16 endmembers, representing different coniferous and deciduous tree crowns and a large range of background materials, was created directly from the image. After applying the ISMA, the abundances of all deciduous crown endmembers were added up. Illuminated pure deciduous crowns were defined as pixels where the combined crown abundance exceeds a threshold of 0.8, while the shade proportion is below a threshold of 0.1 (Figure 5A). The approach allowed to successfully separate deciduous tree crowns (displayed in grey) from coniferous trees (in green) and non-forest surfaces (Figure 5C).

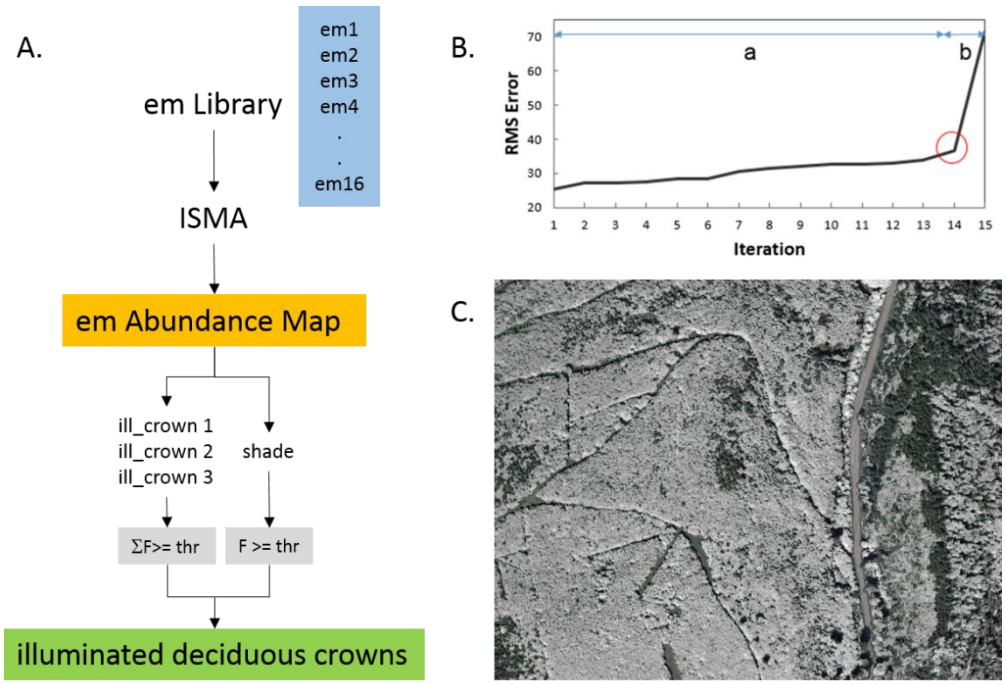

Figure 5. ISMA-based processing chain (**A**) to identify deciduous tree crowns. The identification of the correct endmember set is based on finding the "critical iteration" within the RMSE vector associated with the iterative elimination of spectral endmembers. The red circle marks the critical iteration after which the RMSE increases strongly (**B**). The grey areas in (**C**) are illuminated tree crowns, while the green areas mark the occurrence of coniferous trees.

2.6. Drought-Sensitive Spectral Indices

High temperatures or heat waves combined with precipitation deficits lead to prolonged dry periods and high atmospheric demand for plant transpiration [21,36,50]. Plants may respond to drought and high temperature by closing their stomata, thus reducing their water loss, but eventually facing carbon starvation. The effects on photosynthesis are attributed directly to the stomatal limitations for diffusion of gases and to heat stress, which causes membrane disruption, particularly of thylakoid membranes, and results in a reduced chlorophyll (Chl) content and decreasing light-absorbing efficiency in the photosystems (PSI and PSII). The Chl pigment degradation is commonly observed under drought stress, while plants exposed to high temperatures exhibit reduced Chl biosynthesis [51].

When the stomata are closed to avoid water loss, photosynthesis also depends on the ability to down-regulate PSII activity and safely dissipate excess energy at high-light intensity as heat or

fluorescence. Higher plants typically dissipate 50–70% of all absorbed photons to heat. Reactive photo oxidants are eliminated through a variety of scavenging systems; if the detoxification is not sufficient, the photoproducts will damage the PSII, which leads to photo inhibition [52]. This dissipation process (xanthophyll cycle) is mediated by a particular group of carotenoids located in light harvesting antenna complexes [53]. Under high-light conditions, violaxanthin is converted into zeaxanthin, while at lower light conditions the process is inverted. These conformational changes lead to quenching and heat dissipation. The de-epoxidation process increases the ratio of the total pool of the xanthophyll cycle carotenoids to chlorophyll and, thereby, causes a decrease in leaf reflectance around 531 nm [54]. The maximal degree of conversion to zeaxanthin is observed under exposure to combinations of stress factors; these can also lead to maintaining high levels of zeaxanthin throughout day and night [53].

The extent of these phenomena depends on the species, duration of plant exposure, and stress tolerance, but there is evidence that forest species, such as beech and oak, react in the same way [9]. Especially beech is considered as a relatively drought-susceptible species, which responds to drought stress by a reduction in pre-dawn leaf water potentials, decreased leaf conductance and photosynthesis, and growth reduction [54,55].

As the Donnersberg forest area experienced drought stress since early June (*i.e.*, over 3–4 weeks before data acquisition) one can expect the following effects:

- Reduced chlorophyll concentration (pigment degradation, reduced Chl biosynthesis).
- Changed chlorophyll/carotenoid ratio (xanthophyll cycle).
- Reduced leaf water content (prolonged, excessive transpiration).

Suitable spectral indicators for mapping site-specific tree stress levels should directly relate to these processes. Water absorption features dominate the reflectance of vegetation in the near infrared region (NIR) and SWIR spectral region of the spectrum (900–2500 nm), and numerous studies have demonstrated the linkage between the amount of water in the leaf and specific spectral bands (e.g., [56,57–60]). For single leaves, the water absorption bands in the region 1300–2500 nm showed the highest sensitivity to leaf water concentration [56]. However, due to quick saturation of the signal in the prime absorption regions also weaker absorption bands between 900 and 1300 nm have been considered useful [61,62]. A range of broad- and narrow-band spectral indices has been proposed which are sensitive to water stress in plants [63–69]. For this work, the MSI [66] and the NDWI [64] were selected (Equations (1) and (2)).

$$\mathrm{MSI} = \frac{\rho_{1600}}{\rho_{820}} \quad (1)$$

$$\mathrm{NDWI} = \frac{\rho_{860} - \rho_{1240}}{\rho_{860} + \rho_{1240}} \quad (2)$$

For mapping stress-induced site variations of canopy pigment concentration, two indices were chosen. The PRI (Equation (3)) is sensitive to changes in the chlorophyll/carotenoid ratio, which results from short-term reversible xanthophyll pigment changes associated with plant stress [70–72]. A low PRI indicates reduced photochemical activity of the leaves in response to excess (light-) energy supply and can be interpreted as stress indicator [73]. For estimating chlorophyll content, the chlorophyll index (CI, Equation (4)) which is based on the ratio between NIR and red edge wavelengths [74] was selected; low CI values indicate low chlorophyll content and possible vegetation stress.

$$\text{PRI} = \frac{\rho_{531} - \rho_{570}}{\rho_{531} + \rho_{570}} \quad (3)$$

$$\text{CI} = \left(\frac{\rho_{NIR}}{\rho_{Red\ Edge}}\right) - 1 \quad (4)$$

All indices can be calculated with the "HySpex2.5" and "EnMAP30" data sets. With the simulated Sentinel-2 data ("Sentinel10"), it is possible to calculate the MSI and CI indices, but not the NDWI (no spectral band in the 1240 nm region available). For comparison, a "pseudo-PRI" is defined based on the "Sentinel10"-wavelengths that are next to the originally PRI wavelengths (Table 1); this is not an established index, but useful to test whether Sentinel-2 may provide a comparable stress indicator, although it does not provide exactly the required PRI bandpasses. The MSI has been calculated in its inverted form (*i.e.*, ρ_{820}/ρ_{1600}) to ensure that the index values increase with larger moisture contents.

The MSI, NDWI, and CI incorporate spectral bands from the transmissive near- and shortwave-infrared ranges of vegetation reflectance. This implies that the indices, though efficient at leaf level, are potentially affected by canopy volume and structure (in particular by LAI, fractional cover, background material, but also by atmospheric effects and viewing geometry) (e.g., [69,75–80]). Although the PRI is assumed to be largely decoupled from LAI effects, because it combines only spectral bands from the highly absorptive visible spectral range where leaf transmittance is low, the index is influenced by varying soil background (for LAI < 3) and is sensitive to leaf angle distributions at large viewing angles (>30°) [81].

Table 1. Wavelengths (nm) used for index calculation from the datasets and wavelengths from literature.

Literature	HySpex2.5	EnMAP30	Sentinel10
531	531.3	532.6	490
570	571.3	569.4	560
670	669.7	671.2	665
$\rho_{\text{Red Edge}}$	709.8	711.9	705
ρ_{NIR}	800.9	807.9	783
820	819.1	823.5	842
860	859.2	863.0	865
1240	1243.9	1238.7	---
1600	1598.1	1601.2	1610

2.7. Compensation of Canopy Volume Effects

Although molecular and aerosol scattering effects have been removed (Section 2.4), and the analysis of the "HySpex2.5" data set was constrained to deciduous tree crowns (Section 2.5), a compensation of canopy volume effects was necessary. Colombo *et al.* [75] have suggested to use double ratio indices (which combine the sensitive indices with an index that mainly responds to canopy structure and greenness), assuming that these are correlated to the equivalent water thickness (EWT) and chlorophyll content of the leaves, *i.e.*, the ratios of $\text{EWT}_{\text{canopy}}$/LAI and $\text{CI}_{\text{canopy}}$/LAI. Since traditional greenness indices have no significant correlation with leaf EWT, the Simple Ratio or Reduced Simple Ratio indices (Equations (5) and (6)) might qualify as useful proxies for canopy volume (e.g., [75,82,83]), in particular

because the influence of foliar canopy concentrations of chlorophyll in the visible red spectral region should be of minor importance due to saturation effects within closed deciduous tree crowns (Section 2.5).

$$SR = \frac{\rho_{670}}{\rho_{820}} \quad (5)$$

$$RSR = \frac{\rho_{670}}{\rho_{820}} \cdot \frac{\rho_{1600_{max}} - \rho_{1600}}{\rho_{1600_{max}} - \rho_{1600_{min}}} \quad (6)$$

Alternatively, based on a thorough analysis of the interactions between incoming photons and canopy elements, Knyazikhin *et al.* [84] have defined a "directional area scattering factor" (DASF), which is the directional gap density multiplied by the mean number of interactions before a photon exits the canopy and, therefore, provides a physically based measure of scattering effects of leaves and canopy structure.

The capacity of Simple Ratio (SR), Reduced Simple Ratio (RSR) and DASF to compensate for canopy volume effects, embedded in the selected stress indicators, was analyzed based on simulated canopy spectra, which were generated with the "Invertible Forest Reflectance Model" InFoRM [85–88]. The geometric-optical radiative transfer model InFoRM is a combination of the leaf reflectance models PROSPECT [60,89], the homogeneous canopy model SAILH [90,91], and the forest light interaction model FLIM [92].

With respect to the fact that directional effects in our data set are limited (Section 2.4), and that the stress-related indices were only derived for deciduous tree crowns (Section 2.5), the InFoRM simulation produced 1000 canopy spectra with LAI ranging from 2–5. The remaining model parameters were either fixed or randomly varied within realistic boundaries (Table 2). Results from InFoRM (see Section 3.1) demonstrate that, within the conditions of our data set, the SR and DASF are highly correlated. Since the relationship with LAI seems better defined for the SR than for the DASF, it was decided to use the SR for computing corresponding double ratio indices (DR) (Equation (7)).

$$\mathrm{DRI_{MSI}} = \frac{\mathrm{MSI}}{\mathrm{SR}},\ \mathrm{DRI_{NDWI}} = \frac{\mathrm{NDWI}}{\mathrm{SR}},\ \mathrm{DRI_{CI}} = \frac{\mathrm{CI}}{\mathrm{SR}},\ \mathrm{DRI_{PRI}} = \frac{\mathrm{PRI}}{\mathrm{SR}}. \quad (7)$$

Table 2. Parameter ranges for InFoRM.

Parameter	Symbol	Min	Max
Prospect Structure Parameter	N	1.2	1.6
Chlorophyll a+b (μg cm^{-2})	Cab	30	40
Equivalent Water Thickness (g cm^{-2})	Cw	0.008	0.016
Dry Matter Content (g cm^{-2})	Cm	0.004	0.004
Leaf Area Index	LAI	2	5
Average Leaf Inclination Angle (°)	ALA	30	30
Observation Angle (°)	θo	0	14
Sun Zenith Angle (°)	θs	30	30
Relative Azimuth (°)	ψ	90	90
Stem Density (ha^{-1})	SD	500	1500
Crown Height (m)	H	20	20
Crown Diameter (m)	CD	5	8

For better comparison, all indices were normalized to the range between 0 and 1 using the 0.5 and 99.5 percentiles of the total distribution as lower and upper bounds; these standardized indices were termed MSIn, NDWIn, CIn, PRIn and SRn. The double ratio indices (DRI_{MSI}, DRI_{NDWI}, DRI_{CI}, and DR_{PRI}) were then derived by division through SRn, after the MSIn, NDWIn, CIn, and PRIn histograms were matched to the statistical distribution of SRn (Equation (8)):

$$x_{idxM} = \frac{\sigma_{SRn}}{\sigma_{idx}} x_{idx} + \left(\bar{x}_{SRn} - \frac{\sigma_{SRn}}{\sigma_{idx}} \bar{x}_{idx}\right) \quad (8)$$

where x_{idxM} is the modified index value, σ_{SRn} and $\bar{x}_{SRn}$ are the standard deviation and mean of the reference index (SRn), and σ_{idx} and $\bar{x}_{idx}$ are the standard deviation and mean of the index to be matched to the SRn distribution.

2.8. Statistical Analysis

In order to test whether indices differ significantly between SMCs, analyses of variance (ANOVA) and Tukey's HSD post-hoc tests were carried out. The tests were performed in R, using the functions "aov" for ANOVA and "TukeyHSD" for Tukey's HSD post-hoc test, both included in the "stats" package [93].

The ANOVA reveals only if any class differs from the other classes, requiring a post-hoc test such as the Tukey's HSD to gain further information on which classes can be discriminated. Tukey's HSD test compares the means of all classes pairwise using a studentized range distribution as sampling distribution with the same sample size per class and under consideration of the number of means which are compared. The Tukey HSD post-host test corrects for type I errors, which is necessary for multiple comparisons. The Type I error is the probability to reject a true null hypothesis falsely and is described with the significance level α. Without correction for type I errors, they would cumulate with an increasing number of class comparisons. To retrieve reliable results, a random sample of 100 values per SMC was selected to apply the Tukey's HSD test. This procedure was repeated 100 times and the mean of all *p*-values per class-comparison was calculated. In the "EnMAP30" data set, a sample of 50 values per SMC was selected and the Tukey's HSD test was repeated 100 times, because the number of pixels in the outer soil moisture classes were heavily reduced after being resampled to 30 m.

3. Results

3.1. InFoRM Results

Spectra of InFoRM model results are displayed in Figure 6 left. A comparison with 500 randomly selected image spectra from the "HySpex2.5" data set (Figure 6 right) confirms that the selected model parameters provide a realistic approximation of the spectral variability within the sunlit deciduous tree crowns in our study area.

The simulated crown spectra were used for analyzing the relationship between LAI (as a proxy for canopy volume) and DASF, SR, and RSR. With respect to the conceptual framework of the DASF [84], this seems justified since in our study the structural arrangement of scattering elements is limited to deciduous tree crowns (Section 2.4). Under these conditions, the DASF and SR are highly correlated and both exhibit a significant relationship with LAI; the latter is also true for the RSR but the correlation with

SR and DASF is weak (Figure 7). Since the unifying property of the RSR has been emphasized for mixed forest species, but did not perform equally well for pure deciduous stands [94], it was concluded to use the SR for reducing the influence of canopy volume and structure in the potentially stress-related indices; results for double ratios with RSR and DASF are provided in the supplementary material.

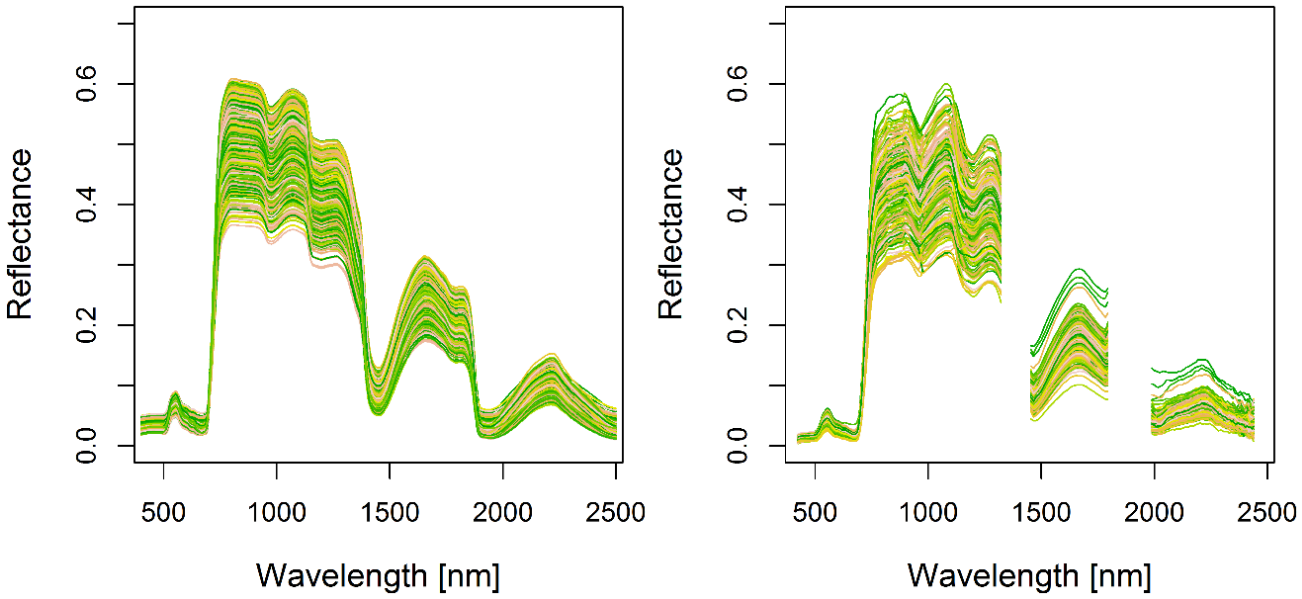

Figure 6. Modelled (**left**) compared to real (**right**) spectra of sunlit deciduous tree crowns.

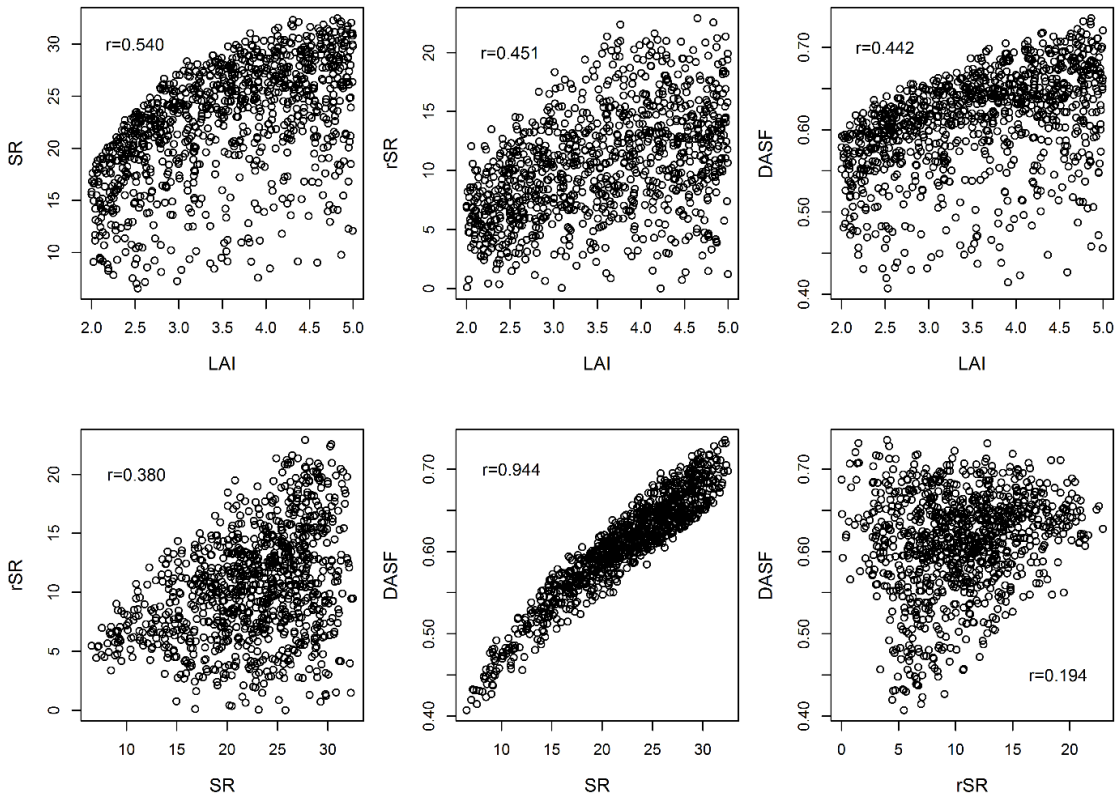

Figure 7. Scatter plots of the relationships between LAI and SR, rSR, and DASF, respectively (**top**), and relationships of the density measures (**bottom**).

3.2. The HySpex2.5 Data Set

3.2.1. Discrimination Analysis

While the correlation between PRIn (expected to be less affected from LAI effects) and all other indices is rather weak, the SRn index (considered a proxy for canopy volume) is moderately correlated with the MSIn (r = 0.41) and, in particular, with the CIn (r = 0.70, Table 3). This suggests that MSIn and CIn represent concentration differences on canopy rather than on leaf level. The water indices MSIn and NDWIn are correlated (r = 0.79), but a considerable part of MSIn variance is not explained by NDWIn.

Table 3. Correlation between the selected spectral indices for the original "HySpex2.5" dataset after eliminating outliers and normalizing all indices in the range 0–1.

HySpex2.5	MSIn	NDWIn	CIn	PRIn	SRn
MSIn	1.00				
NDWIn	0.79	1.00			
CIn	0.39	0.27	1.00		
PRIn	0.31	0.15	0.28	1.00	
SRn	0.41	0.30	0.70	0.12	1.00

The statistical distribution of the PRIn and SRn within each of the SMCs are presented as boxplots (Figure 8). Although the distributions within the SMCs largely overlap, PRIn and SRn have a tendency to increase with improved soil water storage capacities. Figure 8 also shows the averaged *p*-values of the SMC class-comparison derived from Tukey's HSD test for both indices. *P*-values indicate at which significance level indices of two soil moisture classes differ. A high value is emphasized with reddish colors and implies that the index values of the two considered classes cannot be separated. *P*-values with a significance level of 1% are written in bold, a 5% significance level is indicated with underlined digits and a 10% significance level is highlighted in italics. The results suggest that the distribution of the PRIn within SMCs 8 and 9 (very moist/extremely moist) is significantly different from the SMCs 1–4 (moderately to extremely dry) and to some extent even from SMCs 5–7 (moderately moist to moist). The SRn exhibits a similar discrimination capacity: SRn in SMCs 4–9 is significantly different from SMC 1, in SMCs 7–9 from SMCs 2–6, and in SMC 9 from SMCs 1–6. Note that the normalization of PRIn with SR (normalization with DASF and RSR can be found in the supplementary material) has little effect on the *p*-values matrix compared to the canopy volume normalization of water and chlorophyll indices. This intensifies our suggestion that canopy structure and observation geometry has little effect on PRI within the given setup.

Compared to the correlation matrix of the normalized indices (Table 3), the correlation matrix of the double ratios and normalized PRI and SR (Table 4) has changed substantially. It is found that the double-ratioed wetness indices are still highly correlated, but their originally weak correlation with PRIn has now broken down completely. DR_{CI} is neither substantially correlated with DR_{MSI} nor with DR_{NDWI}, although both indices result from the normalization with SRn.

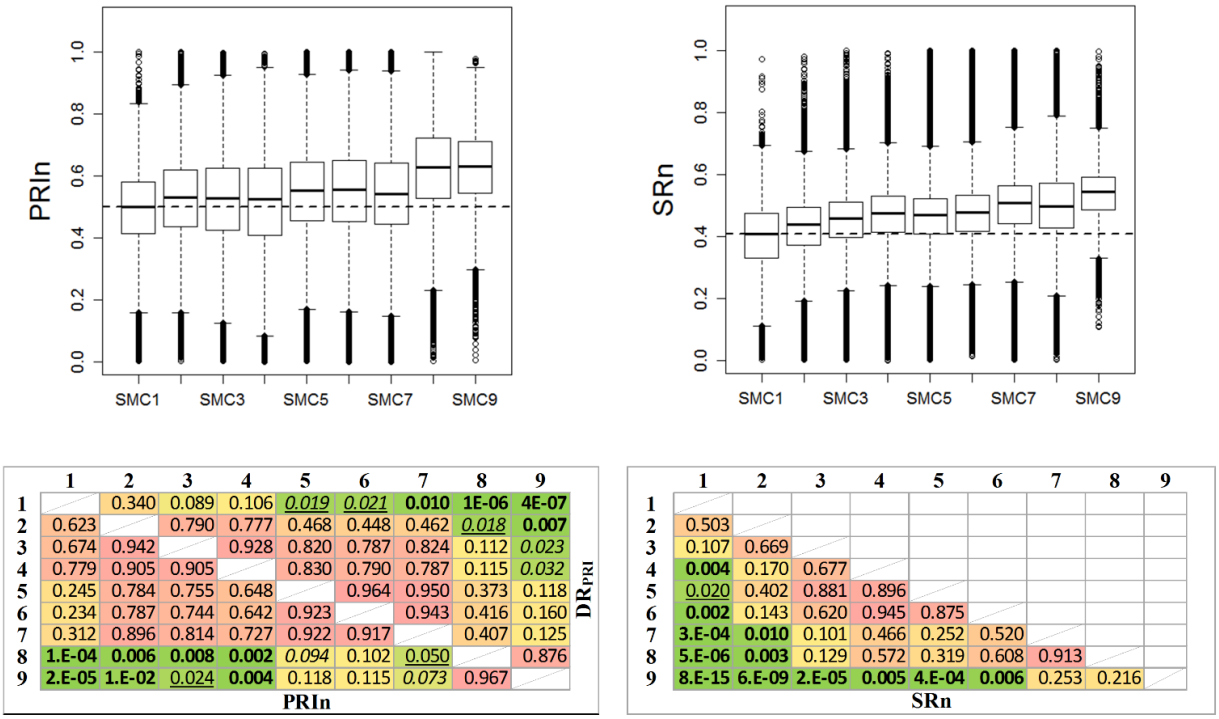

Figure 8. Boxplots of the PRIn and SRn indices per SMC (**top**) and *p*-value matrices of PRIn, DR_{PRI} and SR from Tukey's HSD test for each combination of SMCs (**bottom**); color scheme and character styles emphasize the significance levels (dark green/bold: 1%, green/underlined: 5%, yellow/italics: 10%).

Table 4. Correlation between the selected spectral indices for the original "HySpex2.5" dataset after computing the double ratio indices DR_{MSI}, DR_{NDWI}, and DR_{CI}.

HySpex2.5	DR_{MSI}	DR_{NDWI}	DR_{CI}	PRIn	SRn
DR_{MSI}	1				
DR_{NDWI}	0.66	1			
DR_{CI}	0.13	0.09	1		
PRIn	0.03	0.0004	0.04	1	
SRn	0.27	0.32	0.15	0.01	1

The boxplots of MSIn, NDWIn and CIn exhibit similar characteristics as already described for PRIn and SRn. Although the distributions for each SMC are largely overlapping, one can identify a tendency of the corresponding means to increase with improved soil water storage capacities. However, after computing the double ratios for the water and pigment indices (DR_{MSI}, DR_{NDWI}, DR_{CI}), these trends are completely eliminated (Figure 9).

The results of Tukey's HSD post-hoc test support and further differentiate these findings (Figure 9 Left). The averaged *p*-values in the lower left triangle (comparison between the 0-to-1-normalized distributions) indicate that the MSIn, and particularly the NDWIn, exhibit substantial discrimination capacities. In spite of the large within-class variances, the SMCs 5–9 are significantly different from SMCs 1 and 2, while SMCs 7–9 can still be discriminated from SMC 3 (NDWIn). The MSIn and the CIn behave similarly, although their discrimination capacity is less pronounced.

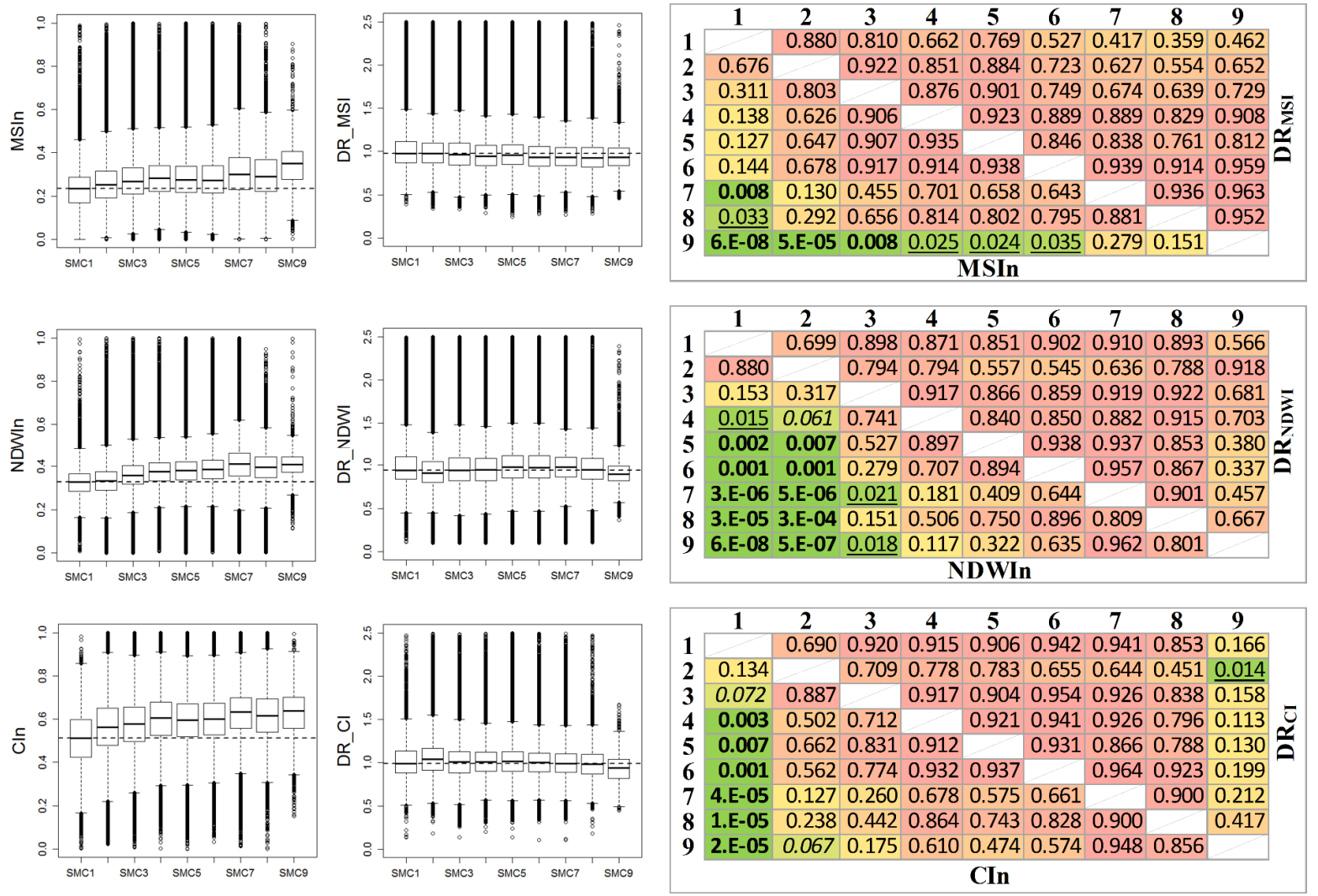

Figure 9. Comparison between SMC-specific boxplots for MSIn, NDWIn, and CIn (**left**; horizontal dashed lines represent the median of the SMC1 distribution) and the corresponding double ratio indices DRMSI, DRNDWI, and DRCI (**center**) and *p*-values (**right**; color scheme and character styles emphasize the significance levels (dark green/bold: 1%, green/underlined: 5%, yellow/italics: 10%)).

3.2.2. Spatial Patterns at the HySpex2.5 Scale

The spatial patterns depicted by PRIn (Figure 10) suggest that photosynthetic stress reactions at the time of the overflight are primarily identified on exposed ridges, mountaintops and steep slopes (preferably with shallow soils and southerly orientation), while plateau areas, lower slopes and valley floors are rather characterized by active photosynthesis. This agrees with the fact that PRI strongly discriminates SMCs with high water storage capacities and stagnant moisture (SMC 8/9) against potentially drier sites (Figure 8), but is less clearly discriminating between the remaining SMCs.

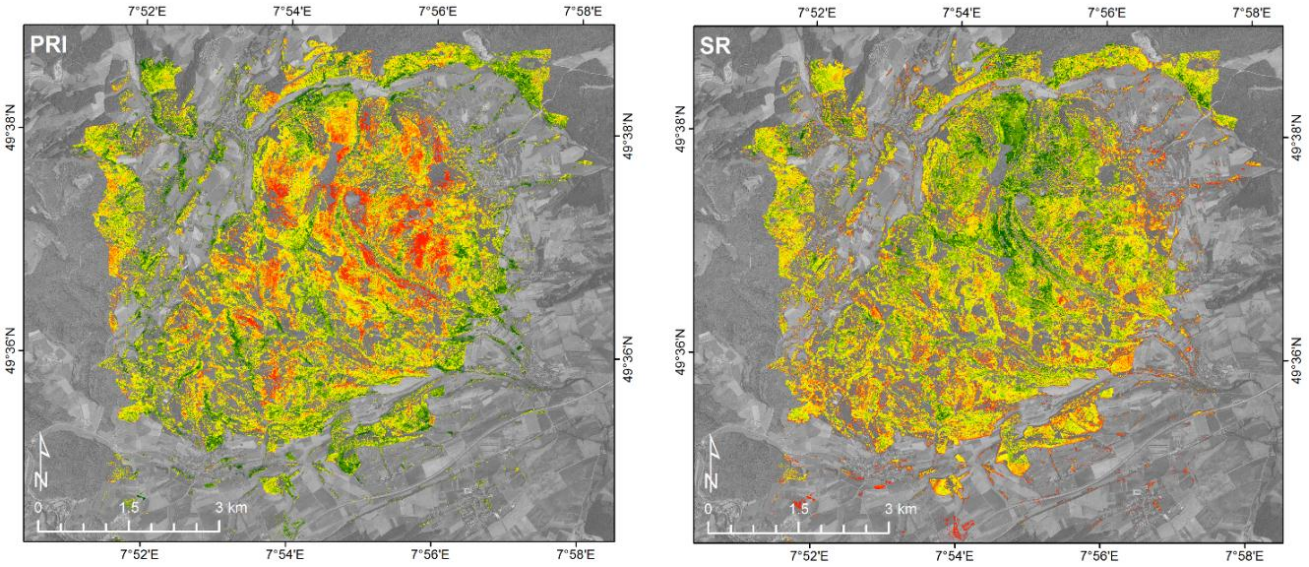

Figure 10. Spatial pattern of PRIn (**left**) and SRn (**right**) produced with the HySpex2.5 data set. All maps are colored from red (mean – 2 standard deviations) to green (mean + 2 standard deviations).

Since the SRn is not correlated with the PRIn (Table 3), the spatial distribution of the SRn scores is different from the PRIn map but in good global agreement with the SMC map (Figure 3). Since average tree-crown height has been shown to increase with more favorable soil moisture regimes (Figure 4), it is strongly suggested that the SRn is intrinsically related to canopy volume and/or biomass.

Due to the high correlation between the MSIn and NDWIn (Table 3), the corresponding maps (Figure 11) display almost identical spatial structures, which to some extent also relate to the relevant spatial structures in the SMC map. The distribution of areas with high and low chlorophyll concentrations in the CIn map, however, show substantial differences to the water-related indices. As already suggested by the poor correlation of the CIn with the MSIn and NDWIn (Table 3), chlorophyll- and water-concentrations are not necessarily coupled (Figure 11). With respect to the growing evidence that SR is representing differences in canopy volume, the resulting double ratio indices (DR_{MSI}, DR_{NDWI} and DR_{CI}) appear much more homogeneously distributed (Figure 11).

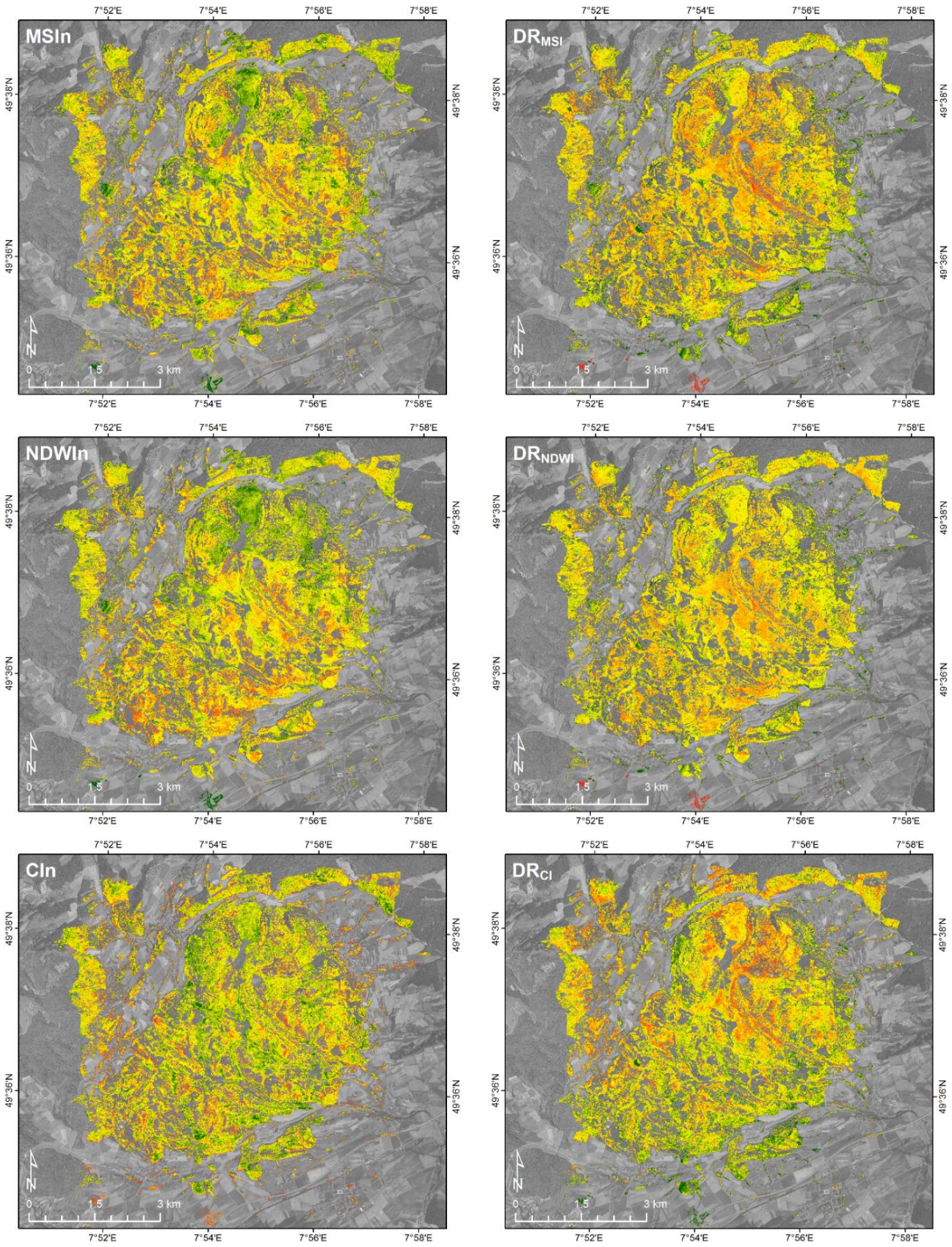

Figure 11. Maps of the normalized water- and chlorophyll-related indices (**left**) in comparison to the corresponding double ratio indices (**right**). All maps are colored from red (mean – 2 standard deviations) to green (mean + 2 standard deviations).

3.3. The EnMAP30 and Sentinel10 Data Sets

For the "Sentinel10" and "EnMAP30" data sets, PRIn ("pseudoPRI" from "Sentinel10" data, compare Section 2.6), DR_{MSI} and DR_{CI} were calculated, and the same statistical analysis was conducted as with the "Hyspex2.5" data (Figure 12).

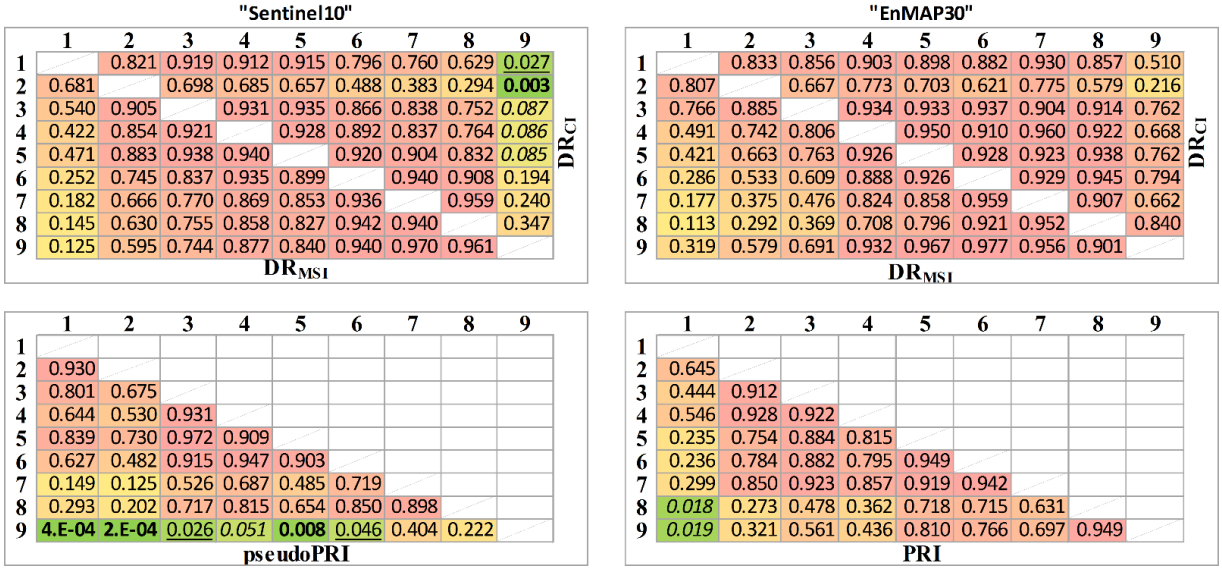

Figure 12. *P*-values for "Sentinel10" DR_{MSI}, DR_{CI}, and "pseudoPRI", (**left**) and "EnMAP30" DR_{MSI}, DR_{CI}, and PRI (**right**). Color scheme and character styles emphasize the significance levels (dark green/bold: 1 %, green/underlined: 5%, yellow/italics: 10%).

"Sentinel10" data *p*-values for "pseudoPRI" show that SMC 9 can be differentiated significantly from the other classes. However, the spatial distribution of "pseudoPRI" in the study area shows no spatial correlation with the SMCs. Therefore, it is assumed that "pseudoPRI" cannot be used to display stress symptoms related to reduced photochemical activity. DR_{MSI} shows that after normalizing MSI with the canopy sensitive SR, SMC pairs cannot be distinguished with a high significance level. DR_{CI} can still be distinguished for class pairs 9-1 and 9-2.

With the "EnMAP30" data set, no class pair can be differentiated significantly with DR_{MSI} and DR_{CI}. For PRI the differences between the classes are extremely small, but class pairs 9-1 and 9-2 can be separated significantly with p values <0.02.

The corresponding maps are displayed in Figure 13. Note that the mask from the stratified HySpex2.5 data set (illuminated tree crowns of beech and oak trees) has been aggregated to 10 m and 30 m pixel size, which lead to different sizes and numbers of data gaps in the maps. The upper two maps show clearly that the "pseudoPRI" does not correlate spatially with the SMCs in the study area, whereas the PRI from "EnMAP30" still shows a good correlation with the SMCs despite the coarser spatial resolution. The maps of DR_{MSI} and especially DR_{CI} from "Sentinel10" seem to overestimate low values (indicating drought stress) in the upper part of the study area where moist SMCs are located, and the corresponding maps from "EnMAP30" show a similar pattern but do not show a spatially distinct image. The double ratio approach and the 30 m resolution lead to a quite homogeneous distribution of DR_{MSI} and DR_{CI}.

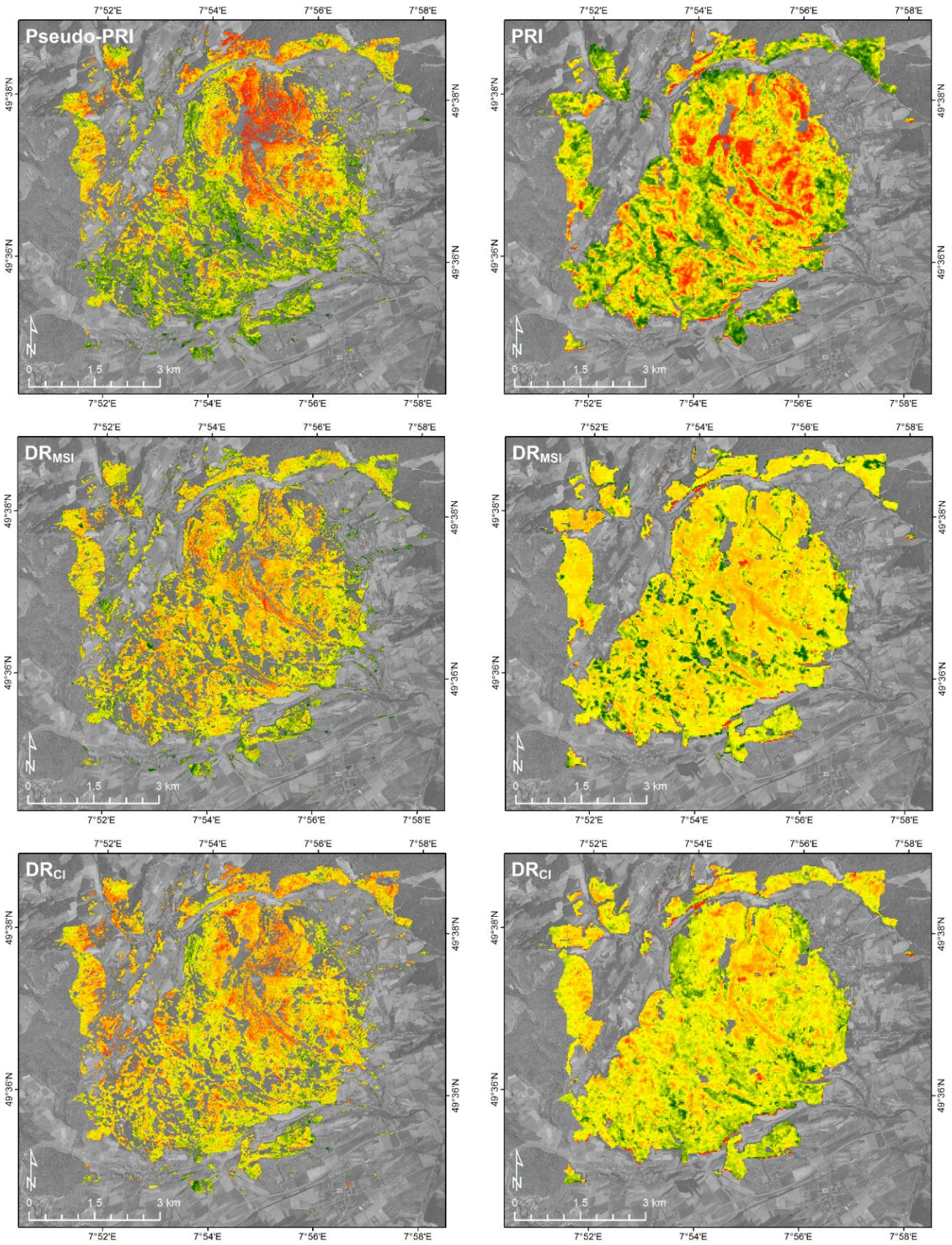

Figure 13. Maps of "pseudoPRI", DR_{MSI} and DR_{CI} from simulated Sentinel-2 data (**left**) and the corresponding indices (PRI, DR_{MSI} and DR_{CI}) from simulated EnMAP data (**right**). All maps are colored from red (mean – 2 standard deviations) to green (mean + 2 standard deviations).

4. Discussion

Although the within-class variance is high in comparison to the inter-class variance of the SMCs, all spectral raw indices computed from the "HySpex2.5" data set have a tendency to increase with improving soil water storage capacities. This correlates with an increase of the CHM-derived tree-height distribution in the SMCs (Section 2.4). However, the computation of all water- and chlorophyll-sensitive indices (MSI, NDWI and CI) involves spectral bands from the NIR and SWIR spectral region, where green vegetation reflectance is substantially influenced by transmission and within-canopy scattering processes. When computing the water- and chlorophyll-related double ratio indices (DR_{MSI}, DR_{NDWI}, DR_{CI}) with respect to the SR or DASF (as a proxy for canopy volume), it is observed that the relationship between elevated water and chlorophyll indicators and increasingly favorable conditions in the SMCs largely disappear. Thus, elevated water and chlorophyll concentrations, as suggested by the raw indices, are primarily correlated with canopy volume and represent an indication of the prevailing site-specific growth conditions but no current stress feature. The spatial pattern in the double ratio indices, assumed to correspond to chlorophyll and water concentration at the leaf level, is no more significantly related to the SMCs. However, it should be understood that the double ratio indices represent "average leaf" conditions. The reason is that the measured reflectance integrates leaf-specific information from upper to lower sections of the crown, and it is well understood that sun-exposed leaves from the upper crown might already exhibit distinct stress phenomena, while shadowed leaves from lower crown sections are still capable of maintaining their normal functioning [95]. This might explain why the mapped gradients of water and chlorophyll concentration at the leaf level, representative for long-term conditions, are not yet particularly sensitive to the different site conditions at this early stage of drought. Furthermore, the assumption of leaf chlorophyll contents being proportional to the degree of drying out cannot be generalized to all types of vegetation [65]. In temperate forests, for example, no correlation was found between the chlorophyll and water content for five different species [96].

The PRI behaves differently. Independently of using the SR or the DASF for compensating canopy scattering effects, the pattern of statistically significant differences between the SMCs is largely maintained with the exception of SMC1, where normalizing the PRI with respect to the SR tends to increase the differences among SMCs 5–7. Since the PRI is related to a spectral range where green leaves are absorbing up to 90% of the incoming radiation, transmission into the canopy is limited to gaps. It should be recalled that larger canopy openings, coniferous trees and shaded parts of the tree crowns had been removed from the "HySpex2.5" data prior to the analysis (Section 2.5). Since the original data set was also acquired under a sun-sensor-target constellation where angular effects are of minor importance, the PRI results are not substantially affected by directional and background effects described by Barton and North (2001) [81] and primarily relate to the sun-exposed upper crown layer. Because of its sensitivity to short-term reversible xanthophyll pigment changes associated with heat and excess light conditions, the PRI is first of all a proxy of plant stress at the time of observation. PRI is also sensitive to water-induced stress conditions on canopy level [73,97,98]. Thus, our results may indicate that the stress reactions are to some extent related to site conditions: maximum stress levels are primarily mapped at sites with low water storage capacities. Since permanent heat stress and water limitation can also lead to maintaining high levels of zeaxanthin throughout day and night [53], it is

also not excluded that the distinct spatial distribution of the PRI represents an expression of site-specific stress conditions inherited from previous days.

In principle, these results are confirmed when transferring the applied processing strategy to simulated EnMAP and Sentinel-2 data. EnMAP in particular has no limitations in producing all tested spectral indices, including the DASF [84] as a physically-based approximation of canopy scattering processes in different stand architectures. However, the main question was whether the reduced spatial resolution (GSD = 30 m) would still allow providing products, which can be related to existing site condition maps. Our results confirm that this is feasible, although the spatial structure of EnMAP data will of course not permit the ISMA-based elimination of canopy gaps to the extent it had been possible in the original data set ("HySpex2.5"). However, with respect to earlier studies (e.g., [99,100]) and the spectral information content provided by EnMAP, one can expect that a successful stratification of forest areas into deciduous and non-deciduous trees will be feasible, such that fundamental canopy differences can be handled efficiently.

This can also be expected from Sentinel-2 data. Although not a subject of this study, it is expected that the improved spatial resolution of Sentinel-2 (GSD = 10 m) might even permit the successful application of suitable unmixing strategies to identify canopy gaps that might contaminate the information about the spectral indices. With its spectral bands in the red-edge region, Sentinel-2 has the spectral coverage to produce the DASF and water- and chlorophyll-related indicators, such as those tested in this study (MSI, CI). In combination with its high repetition frequency, this makes Sentinel-2 highly attractive for monitoring the impact of heat waves and dry spells on forest ecosystems. However, it will be difficult to use the system for observing immediate responses to heat stress and excess light conditions, because the attempt of producing a PRI-compatible indicator by computing a so called "pseudoPRI" using the Sentinel-2 bands closest to the PRI wavebands was not promising.

With respect to the large field-of-view of Sentinel-2, additional processing requirements emerge from the sensitivity of spectral indices to view and illumination angles [101]; EnMAP, when not operating in tilted mode, will be less sensitive to these directional effects. Thus, the results of this study underline the importance of developing concepts for synergetic uses of Sentinel-2 and EnMAP, once both systems will be in operation from 2018 onwards.

5. Conclusions

It was demonstrated that hyperspectral imaging can provide indication on drought- and heat-induced stress levels, which are consistent with the existing site condition maps, both with respect to the long-term impact on water and chlorophyll concentration at the canopy level and the immediate response of already stressed trees to water limitation and excess heat and light conditions. However, the relatively early stage at which the dry spell was observed during summer 2014 did not provide clear indication for site-specific chlorophyll and water deficits at the leaf level. With respect to the use of double ratio indices for compensating canopy volume effects in the reflectance signal, it is suggested to more thoroughly explore the use of physically-based proxies, such as the DASF.

However, PRI was able to display potentially drought induced differences according to the soil moisture regimes. These differences were still visible at the 30m EnMAP resolution, but could not be reproduced with simulated Sentinel-2 data, due to missing spectral bands.

The congruence between SMCs and the spatial pattern of the derived spectral indicators confirmed that these information layers can be used as reference to design more efficient sampling schemes for collecting biophysical data on leaf level. More specifically, statistical evidence and the identified spatial patterns of the PRI suggest how the nine SMCs may be aggregated into three to four meaningful classes. These classes can be used in combination with the PRI map for locating meaningful transects across SMCs where diverse stands can be sampled in a compact area. As highly dynamic biophysical parameters have to be measured within limited time spans, the presented results enable a more efficient sampling strategy, because gradients can be sampled faster as not all nine soil moisture classes have to be considered anymore, and, therefore, more transects can be covered in a shorter time. With this knowledge, impacts of regional warming can be studied efficiently in adequately large and diverse study areas.

Acknowledgments

This research was supported within the framework of the EnMAP project (Contract No. 50 EE 1258) by the German Aerospace Center (DLR) and the German Federal Ministry of Economic Affairs and Energy. The authors thank the state forests Rhineland-Palatinate for providing us the soil moisture regime data and Fliegerclub Region Trier e.V. and our pilot Sven Fischer for his willingness and flexibility in supporting the hyperspectral data acquisition. The authors also acknowledge the support of H.W. Schröck (Forschungsanstalt für Waldökologie und Forstwirtschaft Rheinland-Pfalz) in introducing the authors to the study region and the Rhineland Palatinate "State Bureau of Surveying" (LVermGeo) for providing airborne laser scanning data. Furthermore the authors thank W. Werner (University Trier) for advice on drought stress in Beech stands and evaluation during site-visit. A special thanks goes to Simon Schreiner and Thomas Gattung for their endurance in finding ground control points.

Author Contributions

Sandra Dotzler and Joachim Hill devised the study, wrote the manuscript and did parts of the data processing. Henning Buddenbaum helped in writing and data processing. Johannes Stoffels contributed parts of the data analyses. All authors read and approved the manuscript and contributed figures.

Conflicts of Interest

The authors declare no conflict of interest.

References

1. Boisvenue, C.; Running, S.W. Impacts of climate change on natural forest productivity—Evidence since the middle of the 20th century. *Glob. Change Biol.* **2006**, *12*, 862–882.
2. Field, C.B.; Barros, V.; Stocker, T.F.; Qin, D.; Dokken, D.J.; Ebi, K.L.; Mastrandrea, M.D.; Mach, K.J.; Plattner, G.-K.; Allen, S.K.; *et al. Managing the Risks of Extreme Events and Disasters to Advance Climate Change Adaptation: A Special Report of Working Groups I and II of the Intergovernmental Panel on Climate Change*; Cambridge University Press: Cambridge, UK; New York, NY, USA, 2012.

3. Allen, C.D.; Macalady, A.K.; Chenchouni, H.; Bachelet, D.; McDowell, N.; Vennetier, M.; Kitzberger, T.; Rigling, A.; Breshears, D.D.; Hogg, E.H.; *et al.* A global overview of drought and heat-induced tree mortality reveals emerging climate change risks for forests. *For. Ecol. Manag.* **2010**, *259*, 660–684.
4. European Environment Agency. *Annual Environmental Indicator Report 2012—Ecosystem Resilience and Resource Efficiency in a Green Economy in Europe*; European Environment Agency: Copenhagen, Denmark, 2012.
5. Breda, N. Ground-based measurements of leaf area index: A review of methods, instruments and current controversies. *J. Exp. Bot.* **2003**, *54*, 2403–2417.
6. Beniston, M. The 2003 heat wave in Europe: A shape of things to come? An analysis based on swiss climatological data and model simulations. *Geophys. Res. Lett.* **2004**, doi:10.1029/2003GL018857.
7. Fink, A.H.; Brücher, T.; Krüger, A.; Leckebusch, G.C.; Pinto, J.G.; Ulbrich, U. The 2003 European summer heatwaves and drought—Synoptic diagnosis and impacts. *Weather* **2004**, *59*, 209–216.
8. Lindner, M.; Maroschek, M.; Netherer, S.; Kremer, A.; Barbati, A.; Garcia-Gonzalo, J.; Seidl, R.; Delzon, S.; Corona, P.; Kolström, M.; *et al.* Climate change impacts, adaptive capacity, and vulnerability of European forest ecosystems. *For. Ecol. Manag.* **2010**, *259*, 698–709.
9. Rennenberg, H.; Loreto, F.; Polle, A.; Brilli, F.; Fares, S.; Beniwal, R.S.; Gessler, A. Physiological responses of forest trees to heat and drought. *Plant Biol.* **2006**, *8*, 556–571.
10. Seidl, R.; Schelhaas, M.-J.; Lindner, M.; Lexer, M.J. Modelling bark beetle disturbances in a large scale forest scenario model to assess climate change impacts and evaluate adaptive management strategies. *Reg. Environ. Change* **2009**, *9*, 101–119.
11. Seidl, R.; Schelhaas, M.-J.; Lexer, M.J. Unraveling the drivers of intensifying forest disturbance regimes in Europe. *Glob. Change Biol.* **2011**, *17*, 2842–2852.
12. Schelhaas, M.-J.; Nabuurs, G.-J.; Schuck, A. Natural disturbances in the European forests in the 19th and 20th centuries. *Glob. Change Biol.* **2003**, 1620–1633.
13. Sutmöller, J.; Spellmann, H.; Fiebiger, C.; Albert, M. Der Klimawandel und seine Auswirkungen auf die Buchenwälder in Deutschland—The effects of climate change on beech forests in Germany; In *Beiträge aus der NW-FVA, Band 3*; Universitätsverlag Göttingen: Göttingen, Germany, 2008; pp. 136–158.
14. Reyer, C.; Leuzinger, S.; Ramming, A.; Wolf, A.; Bartholomeus, R.P.; Bonfante, A.; De Lorenzi, F.; Dury, M.; Gloning, P.; Abou Jaoudaé, R.; *et al.* A plant's perspective of extremes: Terrestrial plant responses to changing climatic variability. *Glob. Change Biol.* **2013**, *19*, 75–89.
15. Ciais, P.; Reichstein, M.; Viovy, N.; Granier, A.; Ogée, J.; Allard, V.; Aubinet, M.; Buchmann, N.; Bernhofer, C.; Carrara, A.; *et al.* Europe-wide reduction in primary productivity caused by the heat and drought in 2003. *Nature* **2005**, *437*, 529–533.
16. Vetter, M.; Churkina, G.; Jung, M.; Reichstein, M.; Zaehle, S.; Bondeau, A.; Chen, Y.; Ciais, P.; Feser, F.; Freibauer, A.; *et al.* Analyzing the causes and spatial pattern of the European 2003 carbon flux anomaly using seven models. *Biogeosciences* **2008**, *5*, 561–583.

17. Gobron, N.; Pinty, B.; Mélin, F.; Taberner, M.; Verstraete, M.M.; Belward, A.; Lavergne, T.; Widlowski, J.-L. The state of vegetation in Europe following the 2003 drought. *Int. J. Remote Sens.* **2005**, *26*, 2013–2020.
18. Reichstein, M.; Ciais, P.; Papale, D.; Valentini, R.; Running, S.W.; Viovy, N.; Cramer, W.; Granier, A.; Ogée, J.; Allard, V.; *et al.* Reduction of ecosystem productivity and respiration during the European summer 2003 climate anomaly: A joint flux tower, remote sensing and modelling analysis. *Glob. Change Biol.* **2007**, *13*, 634–651.
19. Hill, J.; Stellmes, M.; Stoffels, J.; Werner, W.; Frantz, D.; Stern, O. Assessing the sensitivity of the European Beech (Fagus sylvatica L.) to drougth stress based on remote measurements from Earth observation satellite. In Proceedings of the 1st EARSeL Forestry Workshop: Operational Remote Sensing in Forest Management, Prague, Czech Republic, 2–3 June 2011; pp. 1–9.
20. Gauer, J.; Feger, K.-H.; Schwärzel, K. Erfassung und Bewertung des Wasserhaushalts von Waldstandorten in der forstlichen Standortskartierung: Gegenwärtiger Stand und künftige Anforderungen. *Waldökologie, Landschaftsforschung und Naturschutz* **2011**, *12*, 7–16.
21. Granier, A.; Reichstein, M.; Bréda, N.; Janssens, I.A.; Falge, E.; Ciais, P.; Grünwald, T.; Aubinet, M.; Berbigier, P.; Bernhofer, C.; *et al.* Evidence for soil water control on carbon and water dynamics in European forests during the extremely dry year: 2003. *Agric. For. Meteorol.* **2007**, *143*, 123–145.
22. Buddenbaum, H.; Stern, O.; Stellmes, M.; Stoffels, J.; Pueschel, P.; Hill, J.; Werner, W. Field imaging spectroscopy of beech seedlings under dryness stress. *Remote Sens.* **2012**, *4*, 3721–3740.
23. Stern, O.; Paschmionka, B.; Stoffels, J.; Buddenbaum, H.; Hill, J. Abbildende und nichtabbildende Geländespektrometrie zur Untersuchung von Stressphänomenen an Buchenpflanzen. The use of imaging and non-imaging spectroscopy for the determination of stress phenomena of beech trees. *Photogramm. Fernerkund. Geoinf.* **2014**, *1*, 17–26.
24. Buddenbaum, H.; Stern, O.; Paschmionka, B.; Hass, E.; Gattung, T.; Stoffels, J.; Hill, J.; Werner, W. Using VNIR and SWIR field imaging spectroscopy for drought stress monitoring of beech seedlings. *Int. J. Remote Sens.* **2015**, *36*, 4590–4605.
25. Buddenbaum, H.; Hill, J. Prospect inversions of leaf laboratory imaging spectroscopy—A comparison of spectral range and inversion technique influences. *Photogramm. Fernerkund. Geoinf.* **2015**, *3*, 231–240.
26. Buddenbaum, H.; Rock, G.; Hill, J.; Werner, W. Measuring stress reactions of beech seedlings with PRI, fluorescence, temperatures and emissivity from VNIR and thermal field imaging spectroscopy. *Eur. J. Remote Sens.* **2015**, *48*, 263–282.
27. Drusch, M.; Del Bello, U.; Carlier, S.; Colin, O.; Fernandez, V.; Gascon, F.; Hoersch, B.; Isola, C.; Laberinti, P.; Martimort, P.; *et al.* Sentinel-2: ESA's optical high-resolution mission for GMES operational services. *Remote Sens. Environ.* **2012**, *120*, 25–36.
28. Guanter, L.; Kaufmann, H.; Segl, K.; Foerster, S.; Rogass, C.; Chabrillat, S.; Kuester, T.; Hollstein, A.; Rossner, G.; Chlebek, C.; *et al.* The EnMAP spaceborne imaging spectroscopy mission for earth observation. *Remote Sens.* **2015**, *7*, 8830–8857.
29. Der Wald in Rheinland-Pfalz: Ergebnisse der Bundeswaldinventur 3. Available online: http://www.wald-rlp.de/fileadmin/website/downloads/bwi3/ergebnispapier_final2.pdf (accessed on 15 May 2015).

30. Running, S.W.; Coughlan, J.C. A general model of forest ecosystem processes for regional applications I. Hydrologic balance, canopy gas exchange and primary production processes. *Ecol. Modell.* **1988**, *42*, 125–154.
31. Running, S.W.; Gower, S.T. FOREST-BGC, a general model of forest ecosystem processes for regional applications. II. Dynamic carbon allocation and nitrogen budgets. *Tree Physiol.* **1991**, *9*, 147–160.
32. Hunt E., Jr.; Martin, F.C.; Running, S.W. Simulating the effects of climatic variation on stem carbon accumulation of a ponderosa pine stand: Comparison with annual growth increment data. *Tree Physiol.* **1991**, *9*, 161–171.
33. Thornton, P.E.; Law, B.E.; Gholz, H.L.; Clark, K.L.; Falge, E.; Ellsworth, D.S.; Goldstein, A.H.; Monson, R.K.; Hollinger, D.; Falk, M.; *et al.* Modeling and measuring the effects of disturbance history and climate on carbon and water budgets in evergreen needleleaf forests. *Agric. For. Meteorol.* **2002**, *113*, 185–222.
34. Buddenbaum, H.; Hientgen, J.; Dotzler, S.; Werner, W.; Hill, J. A BiomeBGC-based evaluation of dryness stress of central European forests. *Int. Arch. Photogramm. Remote Sens. Spat. Inf. Sci.* **2015**, *XL-7/W3*, 345–351.
35. Arbeitskreis Standortskartierung. *Forstliche Standortsaufnahme: Begriffe, Definitionen, Einteilungen, Kennzeichnungen, Erläuterungen*, 6th ed.; IHW Verlag: Eching, Germany, 2003.
36. Bréda, N.; Huc, R.; Granier, A.; Dreyer, E. Temperate forest trees and stands under severe drought: A review of ecophysiological responses, adaptation processes and long-term consequences. *Ann. For. Sci.* **2006**, *63*, 625–644.
37. Hill, J.; Sturm, B. Radiometric correction of multitemporal thematic mapper data for use in agricultural land-cover classification and vegetation monitoring. *Int. J. Remote Sens.* **1991**, *12*, 1471–1491.
38. Tanré, D.; Deroo, C.; Duhaut, P.; Herman, M.; Morcrette, J.J.; Perbos, J.; Deschamps, P.Y. Technical note description of a computer code to simulate the satellite signal in the solar spectrum: The 5S code. *Int. J. Remote Sens.* **1990**, *11*, 659–668.
39. Hill, J.; Mégier, J.; Mehl, W. Land degradation, soil erosion and desertification monitoring in mediterranean ecosystems. *Remote Sens. Rev.* **1995**, *12*, 107–130.
40. Hill, J.; Mehl, W. Geo- und radiometrische Aufbereitung multi-und hyperspektraler Daten zur Erzeugung langjähriger kalibrierter Zeitreihen. *Photogramm. Fernerkund. Geoinf.* **2003**, *1*, 7–14.
41. Schlerf, M.; Atzberger, C.; Hill, J. Remote sensing of forest biophysical variables using HyMap imaging spectrometer data. *Remote Sens. Environ.* **2005**, *95*, 177–194.
42. Schlerf, M.; Atzberger, C.; Hill, J.; Buddenbaum, H.; Werner, W.; Schüler, G. Retrieval of chlorophyll and nitrogen in Norway spruce (Picea abies L. Karst.) using imaging spectroscopy. *Int. J. Appl. Earth Obs. Geoinf.* **2010**, *12*, 17–26.
43. Weber, B.; Olehowski, C.; Knerr, T.; Hill, J.; Deutschewitz, K.; Wessels, D.; Eitel, B.; Büdel, B. A new approach for mapping of biological soil crusts in semidesert areas with hyperspectral imagery. *Remote Sens. Environ.* **2008**, *112*, 2187–2201.
44. Schläpfer, D.; Richter, R. Geo-atmospheric processing of airborne imaging spectrometry data. Part 1: Parametric orthorectification. *Int. J. Remote Sens.* **2002**, *23*, 2609–2630.

45. Buddenbaum, H.; Dotzler, S.; Hill, J. Donnersberg, 2014-07-03—An EnMAP Flight Campaign. GFZ Data Services. 2015. Available online: http://dx.doi.org/10.5880/enmap.2015.006 (accessed on 23 October 2015).
46. Segl, K.; Guanter, L.; Kaufmann, H.; Schubert, J.; Kaiser, S.; Sang, B.; Hofer, S. Simulation of spatial sensor characteristics in the context of the enmap hyperspectral mission. *IEEE Trans. Geosci. Remote Sens.* **2010**, *48*, 3046–3054.
47. Segl, K.; Guanter, L.; Rogass, C.; Kuester, T.; Roessner, S.; Kaufmann, H.; Sang, B.; Mogulsky, V.; Hofer, S. EeteS—The EnMAP end-to-end simulation tool. *IEEE J. Sel. Top. Appl. Earth Obs. Remote Sens.* **2012**, *5*, 522–530.
48. Zarco-Tejada, P.J.; Miller, J.R.; Harron, J.; Hu, B.; Noland, T.L.; Goel, N.; Mohammed, G.H.; Sampson, P.H. Needle chlorophyll content estimation through model inversion using hyperspectral data from boreal conifer forest canopies. *Remote Sens. Environ.* **2004**, *89*, 189–199.
49. Rogge, D.M.; Rivard, B.; Zhang, J.; Feng, J. Iterative spectral unmixing for optimizing per-pixel endmember sets. *IEEE Trans. Geosci. Remote Sens.* **2006**, *44*, 3725–3736.
50. Leuzinger, S.; Zotz, G.; Asshoff, R.; Körner, C. Responses of deciduous forest trees to severe drought in central Europe. *Tree Physiol.* **2005**, *25*, 641–650.
51. Ashraf, M.; Harris, P.J.C. Photosynthesis under stressful environments: An overview. *Photosynthetica* **2013**, *51*, 163–190.
52. Asada, K. The water-water cycle in chloroplasts: Scavenging of active oxygens and dissipation of excess photons. *Ann. Rev. Plant Physiol. Plant Mol. Biol.* **1999**, *50*, 601–639.
53. Demming-Adams, B.; Adams, W.W., III. The role of xanthophyll cycle carotenoids in the protection of photosynthesis. *Trends Plant Sci.* **1996**, *1*, 21–26.
54. Rascher, U.; Nichol, C.J.; Small, C.; Hendricks, L. Monitoring spatio-temporal dynamics of photosynthesis with a portable hyperspectral imaging system. *Photogramm. Eng. Remote Sens.* **2007**, *73*, 45–56.
55. Backes, K.; Leuschner, C. Leaf water relations of competitive fagus sylvatica and quercus petraea trees during 4 years differing in soil drought. *Can. J. For. Res.* **2000**, *30*, 335–346.
56. Carter, G.A. Primary and secondary effects of water content on the spectral reflectance of leaves. *Am. J. Bot.* **1991**, *78*, 916–924.
57. Danson, F.M.; Steven, M.D.; Malthus, T.J.; Clark, J.A. High-spectral resolution data for determining leaf water content. *Int. J. Remote Sens.* **1992**, *13*, 461–470.
58. Aldakheel, Y.Y.; Danson, F.M. Spectral reflectance of dehydrating leaves: Measurements and modelling. *Int. J. Remote Sens.* **1997**, *18*, 3683–3690.
59. Hunt, E.R.; Rock, B.N.; Nobel, P.S. Measurement of leaf relative water content by infrared reflectance. *Remote Sens. Environ.* **1987**, *22*, 429–435.
60. Jacquemoud, S.; Baret, F. Prospect: A model of leaf optical properties spectra. *Remote Sens. Environ.* **1990**, *34*, 75–91.
61. Sims, D.A.; Gamon, J.A. Estimation of vegetation water content and photosynthetic tissue area from spectral reflectance: A comparison of indices based on liquid water and chlorophyll absorption features. *Remote Sens. Environ.* **2003**, *84*, 526–537.
62. Peñuelas, J.; Filella, I.; Biel, C.; Serrano, L.; Savé, R. The reflectance at the 950–970 nm region as an indicator of plant water status. *Int. J. Remote Sens.* **1993**, *14*, 1887–1905.

63. Peñuelas, J.; Pinol, J.; Ogaya, R.; Filella, I. Estimation of plant water concentration by the reflectance water index WI (R900/R970). *Int. J. Remote Sens.* **1997**, *18*, 2869–2875.
64. Gao, B.-C. NDWI—A normalized difference water index for remote sensing of vegetation liquid water from space. *Remote Sens. Environ.* **1996**, *58*, 257–266.
65. Ceccato, P.; Flasse, S.; Tarantola, S.; Jacquemoud, S.; Grégoire, J.-M. Detecting vegetation leaf water content using reflectance in the optical domain. *Remote Sens. Environ.* **2001**, *77*, 22–33.
66. Hunt, E.R.; Rock, B.N. Detection of changes in leaf water content using near and middle-infrared reflectances. *Remote Sens. Environ.* **1989**, *30*, 43–54.
67. Danson, F.M.; Bowyer, P. Estimating live fuel moisture content from remotely sensed reflectance. *Remote Sens. Environ.* **2004**, *92*, 309–321.
68. Datt, B. Remote sensing of water content in eucalyptus leaves. *Aust. J. Bot.* **1999**, *47*, 909–923.
69. Zarco-Tejada, P.J.; Rueda, C.A.; Ustin, S.L. Water content estimation in vegetation with MODIS reflectance data and model inversion methods. *Remote Sens. Environ.* **2003**, *85*, 109–124.
70. Gamon, J.A.; Peñuelas, J.; Field, C.B. A narrow-waveband spectral index that tracks diurnal changes in photosynthetic efficiency. *Remote Sens. Environ.* **1992**, *41*, 35–44.
71. Garbulsky, M.F.; Peñuelas, J.; Gamon, J.; Inoue, Y.; Filella, I. The photochemical reflectance index (PRI) and the remote sensing of leaf, canopy and ecosystem radiation use efficiencies. A review and meta-analysis. *Remote Sens. Environ.* **2011**, *115*, 281–297.
72. Peñuelas, J.; Baret, F.; Filella, I. Semi-empirical indices to assess carotenoids/chlorophyll a ratio from leaf spectral reflectance. *Photosynthetica* **1995**, *31*, 221–230.
73. Suárez, L.; Zarco-Tejada, P.J.; Sepulcre-Cantó, G.; Pérez-Priego, O.; Miller, J.R.; Jiménez-Muñoz, J.C.; Sobrino, J.A. Assessing canopy PRI for water stress detection with diurnal airborne imagery. *Remote Sens. Environ.* **2008**, *112*, 560–575.
74. Gitelson, A.A.; Gritz, Y.; Merzlyak, M.N. Relationships between leaf chlorophyll content and spectral reflectance and algorithms for non-destructive chlorophyll assessment in higher plant leaves. *J. Plant Physiol.* **2003**, *160*, 271–282.
75. Colombo, R.; Meroni, M.; Marchesi, A.; Busetto, L.; Rossini, M.; Giardino, C.; Panigada, C. Estimation of leaf and canopy water content in poplar plantations by means of hyperspectral indices and inverse modeling. *Remote Sens. Environ.* **2008**, *112*, 1820–1834.
76. Dawson, T.P.; Curran, P.J.; North, P.R.J.; Plummer, S.E. The propagation of foliar biochemical absorption features in forest canopy reflectance: A theoretical analysis. *Remote Sens. Environ.* **1999**, *67*, 147–159.
77. Verrelst, J.; Schaepman, M.; Koetz, B.; Kneubühler, M. Angular sensitivity analysis of vegetation indices derived from CHRIS/PROBA data. *Remote Sens. Environ.* **2008**, *112*, 2341–2353.
78. Zarco-Tejada, P.J.; Miller, J.R.; Noland, T.L.; Mohammed, G.H.; Sampson, P. Scaling-up and model inversion methods with narrowband optical indices for chlorophyll content estimation in closed forest canopies with hyperspectral data. *IEEE Trans. Geosci. Remote Sens.* **2001**, *39*, 1491–1507.
79. Zarco-Tejada, P.J.; Miller, J.R.; Morales, A.; Berjón, A.; Agüera, J. Hyperspectral indices and model simulation for chlorophyll estimation in open-canopy tree crops. *Remote Sens. Environ.* **2004**, *90*, 463–476.

80. Daughtry, C.S.T.; Walthall, C.L.; Kim, M.S.; de Colstoun, E.B.; McMurtrey, J.E., III. Estimating corn leaf chlorophyll concentration from leaf and canopy reflectance. *Remote Sens. Environ.* **2000**, *74*, 229–239.
81. Barton, C.V.M.; North, P.R.J. Remote sensing of light use efficiency using the photochemical reflectance index. Model and sensitivity analysis. *Remote Sens. Environ.* **2001**, 264–273.
82. Stenberg, P.; Rautiainen, M.; Manninen, T.; Voipio, P.; Smolander, H. Reduced simple ratio better than NDVI for estimating LAI in finnish pine and spruce stands. *Silva Fenn.* **2004**, *38*, 3–14.
83. Brown, L.; Chen, J.M.; Leblanc, S.G.; Cihlar, J. A shortwave infrared modification of the simple ratio for LAI retrieval in boreal forests: An image and model analysis. *Remote Sens. Environ.* **2000**, *71*, 16–25.
84. Knyazikhin, Y.; Schull, M.A.; Stenberg, P.; Mõttus, M.; Rautiainen, M.; Yang, Y.; Marshak, A.; Carmona, P.L.; Kaufmann, R.K.; Lewis, P. Hyperspectral remote sensing of foliar nitrogen content. *Proc. Natl. Acad. Sci.* **2012**, *110*, E185–E192.
85. Atzberger, C. Development of an invertible forest reflectance model: The INFOR-Model. In *A Decade of Trans-European Remote Sensing Cooperation*, Proceedings of the 20th EARSeL Symposium, Dresden, Germany, 14–16 June 2000; Buchroithner, M., Ed.; **2000**; pp 39–44.
86. Schlerf, M.; Atzberger, C. Inversion of a forest reflectance model to estimate structural canopy variables from hyperspectral remote sensing data. *Remote Sens. Environ.* **2006**, *100*, 281–294.
87. Yuan, H.; Ma, R.; Atzberger, C.; Li, F.; Loiselle, S.A.; Luo, J. Estimating forest fAPAR from multispectral Landsat-8 data using the Invertible Forest Reflectance Model INFORM. *Remote Sens.* **2015**, *7*, 7425–7446.
88. Buddenbaum, H.; Pueschel, P.; Stellmes, M.; Werner, W.; Hill, J. Measuring water and Chlorophyll content on the leaf and canopy scale. *EARSeL eProc.* **2011**, *10*, 66–72.
89. Feret, J.-B.; François, C.; Asner, G.P.; Gitelson, A.A.; Martin, R.E.; Bidel, L.P.R.; Ustin, S.L.; le Maire, G.; Jacquemoud, S. PROSPECT-4 and 5: Advances in the leaf optical properties model separating photosynthetic pigments. *Remote Sens. Environ.* **2008**, *112*, 3030–3043.
90. Verhoef, W. Light scattering by leaf layers with application to canopy reflectance modeling: The sail model. *Remote Sens. Environ.* **1984**, *16*, 125–141.
91. Verhoef, W. Earth observation modeling based on layer scattering matrices. *Remote Sens. Environ.* **1985**, *17*, 165– 178.
92. Rosema, A.; Verhoef, W.; Noorbergen, H.; Borgesius, J.J. A new forest light interaction model in support of forest monitoring. *Remote Sens. Environ.* **1992**, *42*, 23–41.
93. R Development Core Team. *A Language and Environment for Statistical Computing*; R Foundation for Statistical Computing: Vienna, Austria, 2009.
94. Eklundh, L.; Hall, K.; Eriksson, H.M.; Ardö, J.; Pilesjö, P. Investigating the use of landsat thematic mapper for estimation of forest leaf area index in southern sweden. *Can. J. Remote Sens.* **2003**, *29*, 349–362.
95. Hilker, T.; Coops, N.C.; Hall, F.G.; Black, T.A.; Wulder, M.A.; Nesic, Z.; Krishnan, P. Separating physiologically and directionally induced changes in PRI using BRDF models. *Remote Sens. Environ.* **2008**, *112*, 2777–2788.

96. Gond, V.; de Pury, D.G.G.; Veroustraete, F.; Ceulemans, R. Seasonal variations in leaf area index, leaf chlorophyll, and water content; scaling-up to estimate fAPAR and carbon balance in a multilayer, multispecies temperate forest. *Tree Physiol.* **1999**, *19*, 673–679.
97. Dobrowski, S.Z.; Pushnik, J.C.; Zarco-Tejada, P.J.; Ustin, S.L. Simple reflectance indices track heat and water stress-induced changes in steady-state chlorophyll fluorescence at the canopy scale. *Remote Sens. Environ.* **2005**, *97*, 403–414.
98. Evain, S.; Flexas, J.; Moya, I. A new instrument for passive remote sensing: 2. Measurement of leaf and canopy reflectance changes at 531 nm and their relationship with photosynthesis and chlorophyll fluorescence. *Remote Sens. Environ.* **2004**, *91*, 175–185.
99. Stoffels, J.; Hill, J.; Sachtleber, T.; Mader, S.; Buddenbaum, H.; Stern, O.; Langshausen, J.; Dietz, J.; Ontrup, G. Satellite-based derivation of high-resolution forest information layers for operational forest management. *Forests* **2015**, *6*, 1982–2013.
100. Stoffels, J.; Mader, S.; Hill, J.; Werner, W.; Ontrup, G. Satellite-based stand-wise forest cover type mapping using a spatially adaptive classification approach. *Eur. J. For. Res.* **2012**, *131*, 1071–1089.
101. Hilker, T.; Lyapustin, A.; Hall, F.G.; Wang, Y.; Coops, N.C.; Drolet, G.; Black, T.A. An assessment of phyotosynthetic light use efficiency from space: Modeling the atmospheric and directional impacts on PRI reflectance. *Remote Sens. Environ.* **2009**, *113*, 2463–2475.